



CHALMERS
UNIVERSITY OF TECHNOLOGY



Effects of electron trapping and ion collisions on electrostatic shocks

Thesis for the degree of Master of Science in Physics and Astronomy

ANDRÉAS SUNDSTRÖM

Department of Physics
CHALMERS UNIVERSITY OF TECHNOLOGY
Gothenburg, Sweden 2018

Effects of electron trapping and ion collisions on electrostatic shocks

Author:
Andréas Sundström*

Supervisor:
István Pusztai

2018-04-19
Gothenburg, Sweden



DEPARTMENT OF PHYSICS
DIVISION OF SUBATOMIC AND PLASMA PHYSICS
PLASMA THEORY

Effects of electron trapping and ion collisions on electrostatic shocks
ANDRÉAS SUNDSTRÖM

© ANDRÉAS SUNDSTRÖM, 2018.

Supervisor: István Pusztai, Department of Physics
Examiner: Tünde Fülöp, Department of Physics

Department of Physics
Division of Subatomic and Plasma Physics, Plasma theory
Chalmers University of Technology
SE-412 96 Gothenburg
Telephone: +46 (0)31 772 1000

Cover image: Aurora Borealis over Abisko in northern Sweden. Electrostatic shocks have been pointed out as a possible acceleration mechanism that is responsible for accelerating electrons in the solar wind to high enough energy to ionize the gas in the upper atmosphere, creating the glow that is the aurora.

Image © Andréas Sundström, 2018.

Typeset in L^AT_EX
Gothenburg, Sweden 2018

*andsunds@chalmers.se

Effects of electron trapping and ion collisions on electrostatic shocks

Andréas Sundström
Department of Physics
Chalmers University of Technology

Abstract

Electrostatic shocks in plasmas have been observed to be able to accelerate particles to twice the shock velocity with a very low energy spread. Shock phenomena are often modeled as exactly collisionless, which is a very good approximation for astrophysical shocks. However, collisions might play a role in shocks created in laboratory plasmas, since very sharp features of the ion distribution function develop due to ions being reflected at the shock front; this ion reflection results in empty regions of phase space with discontinuities at their boundaries. In this thesis the effects of a weak but finite ion collisionality are considered in a time dependent, semi-analytical treatment. The amplitude of the downstream potential oscillation is found to increase approximately as the square root of time as particles are scattered into the originally empty regions of phase space. The corresponding changes in the electrostatic potential lead to an increased size of the trapping regions in the ion phase space.

This thesis also studies the effect of electron trapping in the potential oscillations downstream of the shockfront. Two model electron distributions, which are flat in the trapped regions of phase space, are considered. The two models only differ in where the potential threshold for trapping is set; one model allows for trapping at a freely set threshold in order to emulate the effects of far downstream behavior of the shock, while the other model only allows for trapping inside the downstream potential oscillation. In general the effects of electron trapping are to reduce the maximum electrostatic potential, but at the same time increase the range of shock propagation speeds for which electrostatic shock solutions exist. The second electron trapping model also exhibits multiple shock solutions for the same temperature ratio and Mach number in certain parameter regions.

Keywords: electrostatic shocks, ion collisions, electron trapping, ion acceleration

Acknowledgment

First and foremost, my gratitude goes to István my supervisor for all the help and useful insights during the whole of this project, either face to face or through the comments on the more than 20 drafts of this thesis. I am especially grateful for the foundational work done by István on the collisional model, without which much of this thesis would not have been where it is today. I would also like to thank Ian and Tünde for useful comments and suggestions on the thesis. Another thank goes to civ.eng., MSc, BSc, herr M. Algehed for giving me the spurring needed to get me to finish this on time. Finally, I would like to thank my family, and especially my beloved father Jan, for always supporting me.

Andréas Sundström, Gothenburg, 2018-04-19

Contents

1	Introduction	1
1.1	What are shockwaves?	2
2	Collisionless shock model	5
2.1	The ion-acoustic wave – a linear wave mode	5
2.1.1	Kinetic theory	5
2.1.2	The Vlasov equation	6
2.1.3	Fluid equations	8
2.1.4	Dispersion of linear ion-acoustic waves	10
2.2	Solitons – initiating the theory of non-linear waves	12
2.2.1	The Sagdeev pseudo-potential	14
2.2.2	Mach number	16
2.2.3	The soliton solution	16
2.2.4	Infinite wavelength	17
2.3	Shockwaves	18
2.3.1	Trapped electrons	23
3	Effects of electron trapping on collisionless shocks	25
3.1	Numerical implementation	25
3.2	Numerical results	27
4	Weakly collisional shocks	33
4.1	Collisions and collision operators	33
4.1.1	Model collision operator for electrostatic shocks	34
4.2	Introducing a small collisionality	35
4.2.1	Perturbative solution with orbit-time-averaging	37
4.2.2	Calculating the orbit-time-averaged squared velocity	39
4.2.3	Arriving at a regular diffusion equation	41
4.2.4	The density of diffused ions	43
4.3	Studying the new variable	45
4.3.1	Asymptotic expansions for $w(\varepsilon)$	45
4.3.2	Returning to the original variables – numerical approach	47
4.3.3	A posteriori verification of previous assumptions	48

4.4 Numerical implementation	49
4.5 The effects of collisions	49
4.6 Possible extensions and improvements	52
5 Conclusions	55
Bibliography	57

Appendix

A Other shock properties	A1
A.1 Ion reflection	A1
A.2 Wavelength	A2

Chapter 1

Introduction

Electrostatic shocks in plasmas are known to be able to accelerate charged particles [1–3], in particular ions. Shock acceleration is somewhat similar to a golf club hitting a golf ball; when the propagating shockwave hits an ion, the ion can bounce off of the shock front with twice the speed of the shockwave. Using high intensity lasers to generate the shocks, this shock acceleration has been observed to produce accelerated protons with an extremely narrow energy spread [4]. This can potentially be used to create compact ion accelerators, with applications in e.g. ion radiation therapy for cancer treatment.

Apart from laboratory plasmas here on earth, shocks are also common in astrophysical plasmas [5–7], where they play an important role in accelerating particles. For instance, shocks have been pointed out as an acceleration mechanism for generating the electrons that cause the aurora [8]. While space plasmas are so tenuous that they can very well be approximated as collisionless, more dense lab plasmas may require a treatment considering the effects of inter-particle collisions; which is why a basic collisional shock model is developed in this thesis. Collisions in electrostatic shocks have also been shown in simulations to cause extremely fast ion heating [9], with possible applications in inertial confinement fusion.

The purpose of this thesis is to develop and investigate semi-analytical models of these types of shocks. These models are developed as extensions of the work done by Cairns et al. [10,11] and by Pusztai et al. [12]. While these shocks can be simulated using kinetic Vlasov solvers or PIC (particle in cell) methods, the benefits of a semi-analytical model lies in the relatively cheap computational cost of running these models. Furthermore, a semi-analytical model can also aid in the understanding of these phenomena due to the freedom to choose input parameters in a way that is not possible in a first-principles simulation.

In this thesis a semi-analytical, kinetic model of electrostatic shocks is presented, and then extended to also account for trapping of electrons and ion collisions. This thesis will begin by first presenting a short introduction to shocks. Thereafter chapter 2 starts with some basic plasma physics. Then, a short study of solitons as examples of non-linear waves is used to lead up to the basic model for the collisionless electrostatic shock. With the shock framework established, the shock model is extended to account for electron

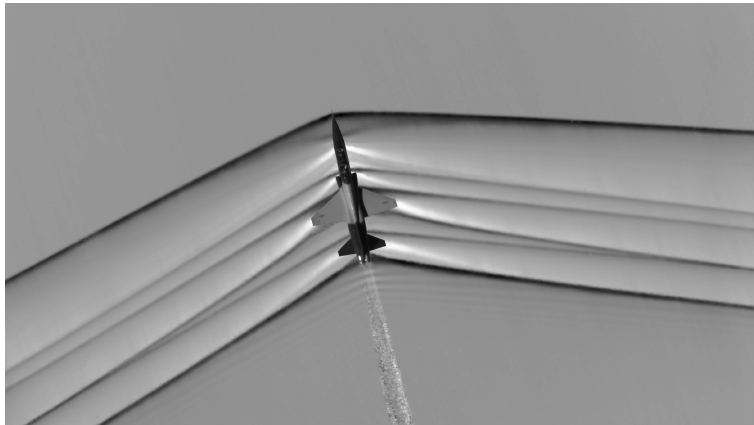


Image credit: NASA.

Figure 1.1: Schlieren image of a fighter jet in supersonic flight with accompanying shockwaves. There are several shockwaves in this photograph, seen as dark bands, from different parts of the aircraft disturbing the air flow enough to create a shock.

trapping; the effects of which are then studied numerically in chapter 3. After that, the new shock model, with a small collisionality, is developed and studied in chapter 4, before the final conclusions are drawn in chapter 5.

1.1 What are shockwaves?

The perhaps best known example of a shockwave is the “sonic boom” produced by a supersonic fighter jet. An example of which is shown in Figure 1.1; the photograph is taken using a method called Schlieren photography, where fluid density variations are made visible as different brightnesses on the image. Each dark streak corresponds to one shock front where the air is greatly compressed.

In a more general sense, shockwaves are wave structures that propagate through a fluid faster than the speed of sound in the fluid – the propagation is *supersonic*. A shockwave is also characterized by having a very thin boundary layer where the fluid pressure varies sharply [13]. It is this steep variation that is the reason for the loud “bang” from a supersonic jet.

The cause of a shockwave can be intuitively understood through the idea of the propagation of information through the fluid via soundwaves. Information about a subsonic disturbance can be transmitted, with soundwaves, to any part of the flow¹; therefore the upstream flow can be “warned” of the obstacle and can thus flow around the obstacle more or less smoothly. If on the other hand the flow is supersonic, the soundwaves are not fast enough to travel upstream to warn about the disturbance, and so the fluid is “shocked” as it abruptly encounters the obstacle. Since the speed of sound is the lower limit for shocks to form, the so called *Mach number* $\mathcal{M} = V/c_s$, named after Ernst Mach, is introduced, where V is the flow speed and c_s is the speed of sound. Shocks can therefore only form at

$\mathcal{M} \geq 1$. The aircraft in Figure 1.1 is flying at $\mathcal{M} = 1.05$.

One thing worth pointing out here is that it need not be *sound waves* per se that mediate the information of the disturbance, but rather any type of information carriers. Regular soundwaves happen to be the culprit in the common examples. This has therefore influenced the terminology. Terms like the *speed of sound* should therefore rather be thought of as the *speed of information propagation* in the fluid.

As an example of a shockwave not mediated by soundwaves, besides the electrostatic shocks of this thesis, consider cars “flowing” down a highway. There, so called traffic waves can occur. They are waves in the car-density arising from the non-zero reaction time of the drivers. One such wave can be observed after a red light turns green; the first car starts accelerating, then the second car shortly thereafter, and so on. Viewed from above this looks like a *wave* of low density propagating backwards through the line of cars. If the car-density, through some random fluctuation, spontaneously rise above a critical density, then this disturbance will continue to grow into what some have called shockwaves [14].

The speed of information is often determined by some linear, low amplitude wave propagation speed. For a wave to be linear, it means that it can mathematically be rescaled and superimposed onto some other linear wave, and still constitute a solution to the (linear) wave equation of the system. Shockwaves, on the other hand, are inherently *non-linear* [15]. For one thing, they propagate faster than the linear waves, so they cannot be described as a linear combination of those waves. This also means that they do not have the same freedom mathematically as linear waves; a shock solution cannot have an arbitrary amplitude for instance. Shockwaves do also often have a larger amplitude than the naturally occurring linear waves; this is because a linear wave theory is often just a low amplitude approximation of some non-linear phenomenon in nature.

In a plasma, a possible linear wave propagating information is the *ion-acoustic* wave. Unlike the electromagnetic waves, which most people are familiar with, the ion-acoustic wave is a longitudinal wave. They stem from longitudinal ion density oscillations in a plasma, which is why they are called ion-acoustic. Since these waves are also electric, they do not require close contact between particles – the electric field is long-range. This also explains why shock structures can be formed, even in tenuous space plasmas.

¹When talking about shocks, it is usually easier to speak of them in their own rest frame. There, the fluid is seen as supersonically flowing towards the shock.

Chapter 2

Collisionless shock model

The electrostatic shocks are studied with a kinetic model based around the idea that the shockwaves reflect ions back upstream. To arrive at this model, a short review of kinetic and linear theory is first presented. Then, solitons are presented as a precursor to the shock model. The shock model is then later modified to take electron trapping into account.

2.1 The ion-acoustic wave – a linear wave mode

Before delving into the non-linear waves, it is instructive to begin by studying some linear wave modes. This will introduce some useful concepts, as well as provide a good review of the basics in plasma physics; for a more in-depth treatment the reader is advised to a proper text book on the subject, e.g. the one by Chen [16].

2.1.1 Kinetic theory

Since plasmas, like regular gases, consist of a very large number of particles, but where each particle interacts electromagnetically, kinetic theory from statistical physics becomes a powerful tool when analyzing plasmas. In kinetic theory it is the one-particle *distribution function*, $f = f(t, \mathbf{x}, \mathbf{v})$, that plays the central role. It gives a measure of the distribution of particles in *phase space*, which consists of all the spacial dimensions as well as the same number of velocity dimensions. Note that the variables \mathbf{x} and \mathbf{v} denote coordinates in phase space, and have nothing to do with any “bulk” or “macro” properties of the plasma.

The interpretation of the distribution function is that $f(t, \mathbf{x}, \mathbf{v}) d^d x d^d v$ gives the number of particles in the phase space volume element $d^d x d^d v$ at the phase space point (\mathbf{x}, \mathbf{v}) at time t , and where d is the number of dimensions considered. This means that the number of particles in a volume $d^d x$ in real space at position \mathbf{x} is given by integrating over all of \mathbf{v} . In other words, the particle number density in real space is

$$n_a(t, \mathbf{x}) = \int_{\text{all } \mathbf{v}} d^d v' f_a(t, \mathbf{x}, \mathbf{v}'), \quad (2.1)$$

where a in this case denotes the particle species (ions or electrons). When more detail is required, the naming convention in this thesis is that subscript “e” denotes electrons, and

“j” denotes any ion species while “i” is reserved for the *main* ion species. The “main ion species” being the ion species with the greatest number of ions, $N_i = \int_{\mathbf{x}} d^d x n_i(x)$; and that usually by far, $N_i \gg N_j$ for $j \neq i$.

In general, a kinetic average of any quantity, χ , can be derived from the distribution function through

$$\langle \chi(t, \mathbf{x}, \mathbf{v}) \rangle_a = \langle \chi \rangle_a(t, \mathbf{x}) = \frac{1}{n_a(t, \mathbf{x})} \int_{\text{all } \mathbf{v}} d^d v' \chi(t, \mathbf{x}, \mathbf{v}') f_a(t, \mathbf{x}, \mathbf{v}'). \quad (2.2)$$

For example, one quite useful average quantity is the bulk flow velocity of a plasma species

$$\mathbf{u}_a(t, \mathbf{x}) = \langle \mathbf{v} \rangle_a = \frac{1}{n_a} \int_{\text{all } \mathbf{v}} d^d v' \mathbf{v}' f_a(t, \mathbf{x}, \mathbf{v}'), \quad (2.3)$$

which will be used later.

The Maxwell-Boltzmann distribution

The Maxwell-Boltzmann distribution function,

$$f_a^{(\text{MB})}(\mathbf{x}, \mathbf{v}) = \frac{n_{a,0}}{(2\pi T_a/m_a)^{d/2}} \exp\left[-\frac{m_a v^2}{2T_a} - Z_a \frac{e\phi(\mathbf{x})}{T_a}\right], \quad (2.4)$$

is the distribution used for non-relativistic particles in thermal equilibrium. Here $v^2 = |\mathbf{v}|^2$, and ϕ is the electrostatic potential; T_a , m_a , Z_a , and $n_{a,0}$ are the temperature, mass, atomic charge number¹, and unperturbed density of species a respectively.

According to (2.1), the particle density of this distribution is

$$n_a^{(\text{MB})}(\mathbf{x}) = n_{a,0} \exp\left[-\frac{eZ_a\phi(\mathbf{x})}{T_a}\right]. \quad (2.5)$$

2.1.2 The Vlasov equation

The distribution function is connected to the number of particles of each species in the system. Therefore, following a phase space trajectory which a particle would follow, the distribution function should be constant along the trajectory as long as there are no collisions². The reason for this is that the number of particles of species a in an infinitesimal phase space volume is $f_a d^d v d^d x$, but since the particles follow precisely this phase space trajectory f_a must be constant along it. That is

$$0 = \frac{d}{dt} [f_a(t, \mathbf{x}(t), \mathbf{v}(t))] = \frac{\partial f_a}{\partial t} + \frac{d\mathbf{x}}{dt} \cdot \frac{\partial f_a}{\partial \mathbf{x}} + \frac{d\mathbf{v}}{dt} \cdot \frac{\partial f_a}{\partial \mathbf{v}}, \quad (2.6)$$

¹That is, the charge of a particle of species a is $Z_a e$, where e is the magnitude of the elementary charge. For an electron $Z_e = -1$.

²At least in the processes relevant for this thesis, where recombination/ionization or nuclear reactions are not present.

where d/dt denotes the total time derivative along the phase space trajectory. This is called the *Vlasov equation*. This equation can be understood more intuitively as a continuity equation in phase space, where the last two terms represent the influx of f_a into an infinitesimal phase space volume, and the partial time derivative is the corresponding rate of change inside this piece of phase space volume. A derivative with respect to a vector is to be understood as a vector of derivatives with respect to each component, i.e. a gradient in the variables of the vector, e.g.

$$\frac{\partial}{\partial \mathbf{x}} = \left(\frac{\partial}{\partial x}, \frac{\partial}{\partial y}, \frac{\partial}{\partial z} \right) = \nabla_{\mathbf{x}}, \quad (2.7)$$

for $\mathbf{x} = (x, y, z)$.

The Vlasov equation can be further rewritten by using

$$\frac{d\mathbf{x}}{dt} \equiv \mathbf{v} \quad \text{and} \quad \frac{d\mathbf{v}}{dt} \equiv \mathbf{a}_a. \quad (2.8)$$

The acceleration, \mathbf{a}_a , can then be written using Newton's second law, and the expression for the Lorentz force acting on a charged particle, as

$$\frac{d\mathbf{v}}{dt} = \frac{1}{m_a} \mathbf{F}_a = \frac{Z_a e}{m_a} (\mathbf{E} + \mathbf{v} \times \mathbf{B}). \quad (2.9)$$

With this, the Vlasov equation becomes

$$\frac{\partial f_a}{\partial t} + \mathbf{v} \cdot \frac{\partial f_a}{\partial \mathbf{x}} + \frac{Z_a e}{m_a} (\mathbf{E} + \mathbf{v} \times \mathbf{B}) \cdot \frac{\partial f_a}{\partial \mathbf{v}} = 0, \quad (2.10a)$$

which is then coupled to Maxwell's equations

$$\begin{aligned} \nabla \cdot \mathbf{E} &= \frac{\rho}{\epsilon_0}, & \nabla \times \mathbf{E} &= -\frac{\partial \mathbf{B}}{\partial t}, \\ \nabla \cdot \mathbf{B} &= 0, & \nabla \times \mathbf{B} &= \mu_0 \mathbf{J} + \mu_0 \epsilon_0 \frac{\partial \mathbf{E}}{\partial t}, \end{aligned} \quad (2.10b)$$

with

$$\rho = e \sum_a Z_a n_a(t, \mathbf{x}) \quad \text{and} \quad \mathbf{J} = e \sum_a Z_a \mathbf{u}_a(t, \mathbf{x}) n_a(t, \mathbf{x}), \quad (2.10c)$$

where the sum is over all particle species – also including electrons using the convention that $Z_e = -1$. In theory, this describes the whole physical system, and is called the Vlasov-Maxwell system of equations. Note that this is a non-linear system of integro-differential equations, since ρ and \mathbf{J} depend on f_a through n_a and \mathbf{u}_a .

The scope of this thesis is, however, limited to non-relativistic systems in which the magnetic field does not affect the dynamics; either where $\mathbf{B} = 0$ or, in some space plasmas, where $\mathbf{v} \parallel \mathbf{B}$. In both cases $\mathbf{v} \times \mathbf{B} = \mathbf{0}$. The system of equations can then be reduced to

$$\frac{\partial f_a}{\partial t} + \mathbf{v} \cdot \frac{\partial f_a}{\partial \mathbf{x}} - \frac{Z_a e}{m_a} \nabla \phi \cdot \frac{\partial f_a}{\partial \mathbf{v}} = 0, \quad (2.11a)$$

and

$$-\nabla^2\phi = \frac{\rho}{\epsilon_0} = \frac{e}{\epsilon_0} \sum_a Z_a n_a(t, \mathbf{x}), \quad (2.11b)$$

where ϕ is the electrostatic potential, and $\mathbf{E} \equiv -\nabla\phi$. This system is called the *Vlasov-Poisson* system of equations, and is the framework in which the electrostatic shocks will be studied in this thesis.

2.1.3 Fluid equations

While the equations (2.10) or (2.11) fully describe the physical system, they can also be hard to work with due to their high dimensionality. Therefore, a fluid moment approach is sometimes used instead. A set of fluid equations can sometimes be sufficient to capture all the essential physics, and at the same time can be much easier to handle and understand intuitively. These fluid equations can be derived from the Vlasov equation (2.10a) through the method of moments, which is based on the kinetic average (2.2).

Given the equation (2.10a), it is clear that multiplying its LHS by some function of only \mathbf{v} , $\chi = \chi(\mathbf{v})$, and integrating over the whole velocity space will still yield zero on the RHS, i.e.

$$\int_v d^d v' \chi(\mathbf{v}') \left[\frac{\partial f_a}{\partial t} + \mathbf{v}' \cdot \frac{\partial f_a}{\partial \mathbf{x}} + \frac{1}{m_a} \mathbf{F}_a \cdot \frac{\partial f_a}{\partial \mathbf{v}'} \right] = 0, \quad (2.12)$$

where $\mathbf{F}_a = Z_a e (\mathbf{E} + \mathbf{v}' \times \mathbf{B})$ for short. For the first term, the time derivative can be moved outside the integration since $\chi(\mathbf{v})$ *only* depends on the phase space coordinate \mathbf{v} , hence

$$\int_v d^d v' \chi(\mathbf{v}') \frac{\partial f_a}{\partial t} = \frac{\partial}{\partial t} \int_v d^d v' \chi(\mathbf{v}') f_a(t, \mathbf{x}, \mathbf{v}') = \frac{\partial}{\partial t} [n_a(t, \mathbf{x}) \langle \chi \rangle_a]. \quad (2.13)$$

The second term is completely analogous,

$$\int_v d^d v' \chi(\mathbf{v}') \mathbf{v}' \cdot \frac{\partial f_a}{\partial \mathbf{x}} = \frac{\partial}{\partial \mathbf{x}} \cdot \int_v d^d v' \chi(\mathbf{v}') \mathbf{v}' f_a(t, \mathbf{x}, \mathbf{v}') = \frac{\partial}{\partial \mathbf{x}} [n_a(t, \mathbf{x}) \langle \chi \mathbf{v} \rangle_a]. \quad (2.14)$$

For the third term, the integration is a bit more involved since the derivative this time is with respect to the integration variable \mathbf{v}' . It can however be done through integration by parts

$$\begin{aligned} \int_v d^d v' \chi(\mathbf{v}') \mathbf{F}_a \cdot \frac{\partial f_a}{\partial \mathbf{v}'} &= \oint_{v \rightarrow \infty} \chi(\mathbf{v}') f_a(t, \mathbf{x}, \mathbf{v}') \mathbf{F}_a \cdot d\mathbf{S} \\ &\quad - \int_v d^d v' f_a(t, \mathbf{x}, \mathbf{v}') \frac{\partial}{\partial \mathbf{v}'} \cdot [\chi(\mathbf{v}') \mathbf{F}_a]. \end{aligned} \quad (2.15)$$

It is again stressed that \mathbf{x} and \mathbf{v} (\mathbf{v}') denote phase space coordinates, and are thus independent of each other. The first integral is a surface integral over the surface where $v \rightarrow \infty$; for any physical system with finite energy $f_a(t, \mathbf{x}, \mathbf{v}) \rightarrow 0$ as $v \rightarrow \infty$, meaning that the surface integral vanishes. For the remaining integral the derivative can be expanded to

$$\frac{\partial}{\partial \mathbf{v}'} \cdot [\chi(\mathbf{v}') \mathbf{F}_a] = \frac{\partial \chi}{\partial \mathbf{v}'} \cdot \mathbf{F}_a + \chi(\mathbf{v}') \frac{\partial}{\partial \mathbf{v}'} \cdot \mathbf{F}_a. \quad (2.16)$$

When substituting in the expression for the Lorentz force,

$$\mathbf{F}_a = \mathbf{F}_a(t, \mathbf{x}, \mathbf{v}') = Z_a e \left(\mathbf{E}(t, \mathbf{x}) + \mathbf{v}' \times \mathbf{B}(t, \mathbf{x}) \right), \quad (2.17)$$

the last term in (2.16) vanishes as

$$\frac{\partial}{\partial \mathbf{v}'} \cdot \left[\mathbf{E}(t, \mathbf{x}) + \mathbf{v}' \times \mathbf{B}(t, \mathbf{x}) \right] = \mathbf{B}(t, \mathbf{x}) \cdot \left(\frac{\partial}{\partial \mathbf{v}'} \times \mathbf{v}' \right) = 0. \quad (2.18)$$

Therefore, what is left of (2.15) is

$$\int_{\mathbf{v}} d^d v' \chi(\mathbf{v}') \mathbf{F}_a \cdot \frac{\partial f_a}{\partial \mathbf{v}'} = - \int_{\mathbf{v}} d^d v' f_a(t, \mathbf{x}, \mathbf{v}') \mathbf{F}_a \cdot \frac{\partial \chi}{\partial \mathbf{v}'} = n_a(t, \mathbf{x}) \left\langle \mathbf{F}_a \cdot \frac{\partial \chi}{\partial \mathbf{v}'} \right\rangle_a, \quad (2.19)$$

which finally gives

$$m_a \frac{\partial}{\partial t} \left[n_a \langle \chi \rangle_a \right] + m_a \frac{\partial}{\partial \mathbf{x}} \cdot \left[n_a \langle \chi \mathbf{v} \rangle_a \right] = e Z_a n_a \left\langle \left(\mathbf{E} + \mathbf{v}' \times \mathbf{B} \right) \cdot \frac{\partial \chi}{\partial \mathbf{v}'} \right\rangle_a \quad (2.20)$$

from (2.12).

The method of moments is to set $\chi(\mathbf{v}) = 1, \mathbf{v}, \mathbf{v}^2, \mathbf{v}^3$ etc., where the higher orders of \mathbf{v} are dyadic vector multiplications also known as outer products, which in tensor index notation is $(\mathbf{v}^\ell)_{k_1, k_1, \dots, k_\ell} = v_{k_1} v_{k_2} \dots v_{k_\ell}$. Each moment, corresponding to setting $\chi(\mathbf{v}) = \mathbf{v}^k$, gives a new equation but also introduces a new variable. Take, for instance, the first two moments. Setting $\chi = 1$ in (2.20), together with (2.3), gives

$$\frac{\partial n_a}{\partial t} + \frac{\partial}{\partial \mathbf{x}} \cdot [n_a \mathbf{u}_a] = 0, \quad (2.21)$$

which is recognized as the continuity equation for the particle density. Then for $\chi = \mathbf{v}$, the calculations become somewhat clearer in tensor index notation³

$$\frac{\partial}{\partial t} [n_a u_{aj}] + \frac{\partial}{\partial x_i} [n_a \langle v'_i v'_j \rangle_a] = \frac{e Z_a n_a}{m_a} \left(E_i + (\mathbf{u}_a \times \mathbf{B})_i \right) \frac{\partial v'_j}{\partial v'_i}. \quad (2.22)$$

Note that the indices i and j in italics are actual indices, whereas i and j in roman font denote different ion species. This can, however, be simplified by setting

$$v'_i = u_{ai} + w_i, \quad (2.23)$$

where w_i is the motion relative to the mean flow velocity, which of course has $\langle w_i \rangle_a = 0$, and

$$\frac{\partial}{\partial x_i} [n_a \langle v'_i v'_j \rangle_a] = \frac{\partial}{\partial x_i} [n_a u_{ai} u_{aj} + n_a \langle w_{ai} w_{aj} \rangle]. \quad (2.24)$$

The second term here is related to the pressure tensor

$$P_{a ij} = m_a n_a \langle w_{ai} w_{aj} \rangle, \quad (2.25)$$

³With the Einstein summation convention that two like indices are summed over, e.g. $r_i s_i = \mathbf{r} \cdot \mathbf{s}$.

which represents the fluid pressure due to the random thermal motion, w_i . This, together with the fact that $\partial v'_j / \partial v'_i = \delta_{ij}$ is the Kronecker delta, results in

$$\frac{\partial}{\partial t} [n_a u_{aj}] + \frac{\partial}{\partial x_i} [n_a u_{ai} u_{aj}] = \frac{e Z_a n_a}{m_a} (E_j + (\mathbf{u}_a \times \mathbf{B})_j) - \frac{1}{m_a} \frac{\partial}{\partial x_i} P_{a ij}. \quad (2.26)$$

The terms on the LHS can be simplified using (2.21), to finally give

$$m_a n_a \frac{\partial u_{aj}}{\partial t} + m_a n_a u_{ai} \frac{\partial u_{aj}}{\partial x_i} = e Z_a n_a (E_j + (\mathbf{u}_a \times \mathbf{B})_j) - \frac{\partial}{\partial x_i} P_{a ij}, \quad (2.27)$$

or in vector notation

$$m_a n_a \frac{\partial \mathbf{u}_a}{\partial t} + m_a n_a \left(\mathbf{u}_{ai} \cdot \frac{\partial}{\partial \mathbf{x}} \right) \mathbf{u}_a = e Z_a n_a (\mathbf{E} + \mathbf{u}_a \times \mathbf{B}) - \frac{\partial}{\partial \mathbf{x}} \cdot \tilde{\mathbf{P}}_a. \quad (2.28)$$

This represents a type of continuity equation for the momentum of the fluid. Together, (2.21), (2.28), and possible higher order moment equations, constitute a *fluid* or *hydrodynamical* system of equations.

The zeroth order moment generated (2.21), which is one equation with two unknowns, n_a and \mathbf{u}_a . Then the next order moment generated another equation for n_a and \mathbf{u}_a , but also introduced the pressure tensor $\tilde{\mathbf{P}}_a$. Hopefully it has become clear that going to the next order moment will not solve this problem. In fact, in theory all the information conveyed by (2.10a) can still be recovered through the method of moments – it just requires infinitely many moments. In practice however, one has to cut off at some point and say that higher order terms of w are negligible compared to the other terms.

2.1.4 Dispersion of linear ion-acoustic waves

A special case, of relevance to the following sections, is the ion-acoustic wave. This wave mode is derived from the cold-ion assumption that ions are much less mobile than the much lighter electrons. Assuming cold ions also means that the random thermal motion of the ions, \mathbf{w}_j , is small and thus the pressure tensor $\tilde{\mathbf{P}}_j$ becomes negligible. The ion-acoustic wave is also an *electrostatic wave mode* meaning that the electric field is longitudinal, i.e. it points in the direction of propagation. Furthermore the plasma is also assumed to be unmagnetized.

To get the equations for the ion-acoustic waves, the fluid equations need to be linearized in terms of a small perturbation

$$\mathbf{E} = \mathbf{E}_0 + \mathbf{E}', \quad n_j = n_{j,0} + n'_j, \quad \text{and} \quad \mathbf{u}_j = \mathbf{u}_{j,0} + \mathbf{u}'_j. \quad (2.29)$$

The unperturbed state is assumed to be static and uniform, meaning that $\mathbf{E}_0 = \mathbf{0}$, $\mathbf{u}_{j,0} = \mathbf{0}$, and $\partial n_{j,0} / \partial \mathbf{x} = \mathbf{0}$. Expanding (2.21) and (2.28) to linear order in the primed variables yields

$$\frac{\partial n'_j}{\partial t} + n_{j,0} \frac{\partial}{\partial \mathbf{x}} \cdot \mathbf{u}'_j = 0, \quad (2.30a)$$

2.1. The ion-acoustic wave – a linear wave mode

and

$$m_j \frac{\partial \mathbf{u}'_j}{\partial t} = e Z_j \mathbf{E}'. \quad (2.30b)$$

The wave mechanics is then best understood through an expansion in terms of plane waves, $e^{i\mathbf{k}\cdot\mathbf{x} - i\omega t}$. Also, since the wave is longitudinal all the information about the wave lies along the direction of wave propagation, parallel to \mathbf{k} . The equations can therefore be simplified to 1D by setting the coordinate system such that $\mathbf{k} = k\hat{\mathbf{x}}$, $\mathbf{u}'_j = u'_j\hat{\mathbf{x}}$, and $\mathbf{E}' = E'\hat{\mathbf{x}}$. The linearized equations now become

$$-i\omega n'_j + ik n_{j,0} u'_j = 0, \quad (2.31a)$$

and

$$-i\omega m_j u'_j = e Z_j E' = -ike Z_j \phi', \quad (2.31b)$$

where $E' = \partial\phi'/\partial x$. For the electrons, which were assumed hot, their density is given by the Maxwell-Boltzmann density (2.5)

$$n_e = n_{e,0} + n'_e = n_{e,0} \exp\left(\frac{e\phi'}{T_e}\right) \approx n_{e,0} \left(1 + \frac{e\phi'}{T_e}\right). \quad (2.32)$$

The potential is given by the Poisson equation (2.11b), which here becomes

$$-\epsilon_0 (ik)^2 \phi = e \left[\sum_j Z_j n_{j,0} - n_{e,0} \right] + e \left[\sum_j Z_j n'_j - n'_e \right]. \quad (2.33)$$

The first bracket vanishes due to the unperturbed plasma being quasi-neutral

$$n_{e,0} = \sum_j Z_j n_{j,0} =: n_0. \quad (2.34)$$

Now, substituting (2.31a) into (2.31b) yields

$$\frac{\omega^2}{k^2} n'_j = n_{j,0} \frac{e Z_j}{m_j} \phi'; \quad (2.35)$$

then, with n'_e from (2.32), (2.33) becomes

$$\left(\frac{\epsilon_0 k^2}{e} + \frac{n_0 e}{T_e} \right) \phi' = e \phi' \frac{k^2}{\omega^2} \sum_j \frac{n_{j,0} Z_j^2}{m_j}. \quad (2.36)$$

This can be simplified to the dispersion relation

$$\frac{\omega^2}{k^2} \left(1 + k^2 \lambda_D^2 \right) = \frac{T_e}{n_0} \sum_j \frac{n_{j,0} Z_j^2}{m_j}. \quad (2.37)$$

where

$$\lambda_D = \sqrt{\frac{\epsilon_0 T_e}{e^2 n_0}} \quad (2.38)$$

is called the *Debye length*. It might also be clear for the reader why this is called the *ion-acoustic* wave. It is because, similarly to a regular sound wave, the oscillation is in the density and flow velocity of the ions, the only difference being that it is the electrostatic interaction between ions which mediates the oscillations. Meanwhile, the electrons just instantaneously follow, without actually contributing to the oscillations.

The Debye length, λ_D , came from the effects of the electrons and their Maxwell-Boltzmann distribution. This length scale arises in many different problems where the electrons are assumed mobile. In such a situation the electrons will react to an electrostatic potential in such a way as to try to counteract or shield the potential. Then, as in this case, the length scales on which this electron shielding acts is the Debye length. In other words, a microscopic fluctuation will be compensated by the shielding electrons, and the plasma will look smooth and neutral on length scales larger than λ_D .

In the long wavelength limit, $k\lambda_D \ll 1$, (2.37) can be written as

$$u_{\text{phase}}^2 = \frac{T_e Z_i}{m_i} \sum_j \frac{Z_j m_i}{m_j Z_i} \frac{Z_j n_{j,0}}{n_0} = c_s^2 \sum_j \zeta_j \frac{Z_j n_{j,0}}{n_0} \quad (2.39)$$

for some ion species denoted with a subscript “i”, and where $u_{\text{phase}} = \omega/k$ is the phase speed of the wave, $\zeta_j := Z_j m_i / (m_j Z_i)$, and

$$c_s := \sqrt{\frac{T_e Z_i}{m_i}} \quad (2.40)$$

is referred to as the ion-acoustic wave propagation speed – or the speed of sound for short. The reason why c_s is called this is that when the “i” ion species is the main ion species, meaning that $Z_i n_{i,0} \gg Z_j n_{j,0}$ for $j \neq i$, then $u_{\text{phase}} \approx c_s$. In a single ion species plasma, $\zeta_i = 1$, $n_0 = Z_i n_{i,0}$, and $u_{\text{phase}} = c_s$ becomes exact.

Finite ion temperature

In the derivation above, the ions were assumed to be cold, i.e. T_j was completely neglected in the fluid description. However, it is possible to include a finite ion temperature; that would give an ion acoustic phase velocity of [17, eq. (6.76)]

$$u_{\text{phase}} = \sqrt{\frac{Z_i T_e + \gamma_i T_i}{m_i}} = c_s \sqrt{1 + \frac{\gamma_i T_i}{Z_i T_e}} \quad (2.41)$$

for a single ion species plasma. The parameter γ_i is analogous to the adiabatic index, also denoted γ , used in thermodynamics.

2.2 Solitons – initiating the theory of non-linear waves

In the example with traffic waves, in section 1.1, the shocks only originate from high-enough amplitude perturbations. Then, for the ion-acoustic waves above, one of the

premises of the whole derivation was that the oscillations be small enough that higher-than-linear terms could be discarded. The fact that non-linear phenomena mostly only show up for high amplitudes is symptomatic of such phenomena. It is often the case, in many physical systems, that a linearized model works well for sufficiently small perturbations – like in the previous section. However, at some point, the linear model breaks down, like for example with Hooke’s law or Ohm’s law – a spring will plastically deform from over-stretching, and a resistor will burn up if too much current is passed through it. These might seem like silly examples, but they are examples of *non-linear* phenomenon nonetheless.

Solitons are like the little brother of shockwaves, both are non-linear waves and both travel faster than their low-amplitude linear cousins, i.e. they are supersonic with respect to the basic wave propagation speed in the medium. It is therefore instructive to begin by studying them briefly, and pick up some useful analytical tools and tricks, before going on to study the shocks. Solitons occur as a phenomenon where linear dispersion effects, which generally broadens pulse features, are balanced by non-linear focusing effects, which act to compress a pulse. The result then becomes a solitary wave which can propagate more or less indefinitely with the same shape throughout its whole path⁴. This is also, in some sense, what sets solitons apart from shocks; solitons are non-dissipative [15, ch. 3], which makes them symmetric in the up- and downstream directions – see Figure 2.2 for an example of how a soliton can look like. This section is based on, and expanded from, the treatment of solitons in chapter 6 of the book by Tidman and Krall [1], wherein they also introduce solitons as a gateway to shocks. This is a very narrow treatment of solitons, suitable for continuing on to electrostatic shocks in plasmas, for a more in-depth treatment of solitons, the reader is encouraged to look up other text on non-linear waves – e.g. Scott [15].

Continuing with the cold ion approximation, $T_i \ll T_e$, in the hydrodynamical system of equations in 1D, The continuity equation is

$$\frac{\partial n_i}{\partial t} + \frac{\partial}{\partial x}[n_i u] = 0, \quad (2.42)$$

and the momentum equation becomes

$$n_i m_i \left[\frac{\partial u}{\partial t} + u \frac{\partial u}{\partial x} \right] = -n_i e Z_i \frac{\partial \phi}{\partial x} \quad (2.43)$$

in the absence of magnetic fields. Here $u = u(x)$ is the bulk flow of the plasma, and is therefore a function of x . Note that this is a non-linear system of equations since there are terms with products of the two unknowns n_i and u , or their derivatives.

The analysis is carried out in the co-moving frame of the soliton, with the x coordinate set such that the soliton is centered around $x = 0$. Focusing on steady state solutions in this frame, the time derivatives can be set to zero, $\partial/\partial t \rightarrow 0$. For (2.42), this results in

⁴It should be pointed out that some circumstances require a more strict differentiation between solitons and solitary waves, due to some different properties in e.g. interactions between waves. In this thesis, the word soliton will be used with more loose definition.

the product $n_i u$ being constant over x , specifically $n_i u = n_{i,0} V$ where $n_{i,0}$ and V represents the values of the respective quantities as $x \rightarrow \pm\infty$, far away from the soliton. Doing the same for (2.43), and noting that $u \partial u / \partial x = \frac{1}{2} \partial(u^2) / \partial x$, yields

$$E = \frac{1}{2} m_i u^2 + e Z_i \phi = \frac{1}{2} m_i V^2, \quad (2.44)$$

where E is of course the energy of an ion. Here ϕ is taken to be zero at $x \rightarrow \pm\infty$. With these two results the ion density can be written as

$$n_i = \frac{n_{i,0} V}{u} = \frac{n_{i,0} V}{\sqrt{V^2 - \frac{2eZ_i}{m_i} \phi}}. \quad (2.45)$$

Assuming that the electrons follow a Maxwell-Boltzmann distribution, (2.4), the electron density becomes

$$n_e = n_{e,0} \exp\left(\frac{e\phi}{T_e}\right), \quad (2.46)$$

according to (2.5), where $n_{e,0}$ is the electron density far away from the soliton, where $\phi = 0$. It is clear from quasi-neutrality considerations that

$$n_{e,0} = Z_i n_{i,0} =: n_0. \quad (2.47)$$

Note that the quasi-neutrality condition only applies to the unperturbed plasma, there must be a net charge density inside the soliton for the potential to change as it does.

It is now possible to use (2.45) and (2.46) to write down Poisson's equation for the electrostatic potential, in a single ion species plasma, as

$$-\frac{d^2 \phi}{dx^2} = \frac{e(Z_i n_i - n_e)}{\epsilon_0} = \frac{e n_0}{\epsilon_0} \left[\frac{V}{\sqrt{V^2 - \frac{2eZ_i}{m_i} \phi}} - \exp\left(\frac{e\phi}{T_e}\right) \right]. \quad (2.48)$$

2.2.1 The Sagdeev pseudo-potential

To get a better understanding of the solution of (2.48), a so called Sagdeev pseudo-potential $\Phi(\phi)$ is introduced. It is defined so that

$$\frac{d^2 \phi}{dx^2} = -\frac{\partial \Phi}{\partial \phi}. \quad (2.49)$$

Begin by noticing the similarity between this one-dimensional Poisson equation and Newton's second law.⁵ Just as in the case of a mechanical system, it is simple to show that this leads to

$$\frac{1}{2} \left(\frac{d\phi}{dx} \right)^2 + \Phi(\phi) = W, \quad (2.50)$$

⁵Think of replacing $x \rightarrow t$, $\phi(x) \rightarrow s(t)$, and $\Phi(\phi) \rightarrow U(s)/m$, where t is the time, s the position of a particle of mass m , and U is the potential well the particle is gliding in. This gives the familiar $m\ddot{s}(t) = -\partial U / \partial s$, which is Newton's second law for a particle moving in a potential, $U(s)$.

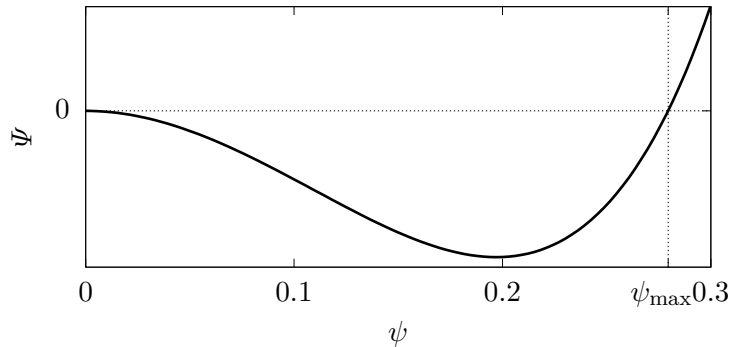


Figure 2.1: An example form of the Sagdeev potential, plotted with the dimensionless parameters $\Psi = \epsilon_0 \Phi / (n_0 T_e)$ and $\psi = e\phi / T_e$. The Sagdeev potential here is for Mach number $\mathcal{M} = 1.1$ with $\mathcal{M} = V/c_s$, where c_s is the ion acoustic wave speed as in (2.40). Note that $\Psi(\psi_{\max}) = 0$ corresponds to ψ_{\max} being the maximum value of the potential of the soliton.

by multiplying both sides of (2.49) with $d\phi/dx$ and integrating over x . The constant of motion, W , stems from the integration, and it would be the total mechanical energy in the analogy. The pseudo-potential Φ is, like in a mechanical system, only determined up to an additive constant. The condition imposed on ϕ , that $\phi(x) \rightarrow 0$ as $x \rightarrow \pm\infty$, also implies that $\partial\phi/\partial x \rightarrow 0$ as $\phi \rightarrow 0$, which is realized by setting $\Phi(\phi) \rightarrow W$ as $\phi \rightarrow 0$. In other words, the constant of integration can be chosen to be $W = 0$, resulting in

$$\frac{1}{2} \left(\frac{d\phi}{dx} \right)^2 + \Phi(\phi) = 0, \quad (2.51)$$

as long as $\Phi(\phi) \rightarrow 0$ as $\phi \rightarrow 0$. In the case of the soliton, (2.48), this would correspond to having

$$\Phi(\phi) = \frac{n_0 T_e}{\epsilon_0} \left[\frac{m_i}{Z_i T_e} \left(V^2 - V \sqrt{V^2 - \frac{2eZ_i}{m_i} \phi} \right) + 1 - \exp\left(\frac{e\phi}{T_e}\right) \right], \quad (2.52)$$

which is obtained by simply integrating the RHS of (2.48) and applying $\Phi(\phi) \rightarrow 0$ as $\phi \rightarrow 0$.

An interpretation of (2.51) is that the solution for $\phi(x)$ can be interpreted as finding the trajectory of an imagined particle gliding, with zero total energy, in the potential $\Phi(\phi)$, like in Figure 2.1. The fact that the electrostatic potential has to obey (2.51) means that the allowed ϕ must satisfy $\Phi(\phi) \leq 0$, which means that the maximum value of the electrostatic potential, ϕ_{\max} , is at the first positive root of $\Phi(\phi_{\max}) = 0$. Another way of seeing this is that (2.51) requires that $\partial\phi/\partial x = 0$ only when $\Phi = 0$, i.e. ϕ has a maximum or a minimum when $\Phi = 0$. This becomes important in the section 2.3, where shock are discussed. The analogy that a particle is gliding back and forth in the Sagdeev potential, $\Phi(\phi)$, also ensures that the soliton is symmetric in the up- and downstream directions.

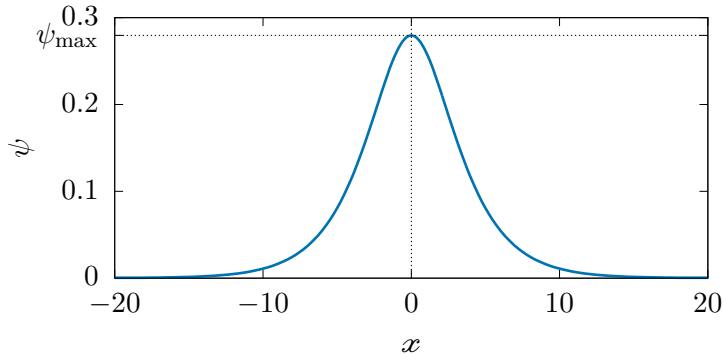


Figure 2.2: The electrostatic potential of a plasma soliton with Mach number $\mathcal{M} = 1.1$. Notice that the indicated maximum value, ψ_{\max} , is the same as is shown in Figure 2.1.

2.2.2 Mach number

The factor $m_i/(Z_i T_e)$ in (2.52) can be recognized as the inverse square of the ion-acoustic wave propagation speed, c_s from (2.40). Without knowing if this is the proper choice, define the Mach number to be

$$\mathcal{M} := \frac{V}{c_s} = \frac{V}{\sqrt{Z_i T_e / m_i}}. \quad (2.53)$$

The Sagdeev potential in (2.52) can now be written as

$$\Psi(\psi) = \frac{\epsilon_0}{n_0 T_e} \Phi(\phi) = \mathcal{M}^2 - \mathcal{M} \sqrt{\mathcal{M}^2 - 2\psi + 1} - e^\psi, \quad (2.54)$$

where the dimensionless parameters Ψ and $\psi = e\phi/T_e$ have been introduced for notational clarity. The shape of $\Psi(\psi)$ at $\mathcal{M} = 1.1$ is plotted in Figure 2.1.

To see that (2.53) is indeed the right choice of Mach number, Taylor expand (2.54) for $\psi \ll 1$, which gives

$$\Psi(\psi) = -\frac{\psi^2}{2\mathcal{M}^2} (\mathcal{M}^2 - 1) + \mathcal{O}(\psi^3). \quad (2.55)$$

Now, notice that (2.51) requires that $\Phi \leq 0$ ($\Psi \leq 0$) for all values of ϕ (ψ). For this to be valid in the limit $\psi \ll 1$, (2.55) requires that the Mach number has to fulfill $\mathcal{M}^2 > 1$, i.e. $|\mathcal{M}| > 1$, which is to be expected of a “proper” Mach number. Furthermore, from (2.45) it is clear the V and u must have the same sign, and since u is taken to be positive, so must V and \mathcal{M} .

2.2.3 The soliton solution

With this Mach number, the Poisson equation for these solitons, (2.48), can be rewritten using \mathcal{M} from (2.53) and $\psi = e\phi/T_e$. To further clean up the equation the new dimensionless coordinate⁶ $x = x/\lambda_D$ is used, with the Debye length λ_D from (2.38). This results

in the dimensionless Poisson equation

$$-\frac{d^2\psi}{dx^2} = \frac{\mathcal{M}}{\sqrt{\mathcal{M}^2 - 2\psi}} - e^\psi. \quad (2.56)$$

Unfortunately this cannot be solved analytically, but a numerical solution for $\mathcal{M} = 1.1$ is shown in Figure 2.2. Also note that since this is a second order ODE, two boundary conditions are required and they are given by

$$\psi(x=0) = \psi_{\max}, \quad \left. \frac{d\psi}{dx} \right|_{x=0} = 0, \quad (2.57)$$

where ψ_{\max} is given by $\Psi(\psi = \psi_{\max}) = 0$.

2.2.4 Infinite wavelength

The fact that the soliton solution is just one single potential hump can be rephrased that it is an oscillation with infinite wavelength. By the analogy of a particle gliding in the pseudo potential, the wavelength of the electrostatic potential oscillation corresponds to the period time it takes this imaginary particle to glide back and forth in the pseudo potential.

The wavelength can be calculated using the normalized version of (2.51),

$$\frac{1}{2} \left(\frac{d\psi}{dx} \right)^2 + \Psi(\psi) = 0. \quad (2.58)$$

Now the normalized wavelength, λ , is given by

$$\lambda = 2 \int_0^{\lambda/2} dx = 2 \int_0^{\psi_{\max}} \left(\frac{d\psi}{dx} \right)^{-1} d\psi = \sqrt{2} \int_0^{\psi_{\max}} \frac{d\psi}{\sqrt{-\Psi(\psi)}}. \quad (2.59)$$

However (2.55) says that

$$\frac{1}{\sqrt{-\Psi(\psi)}} \propto \frac{1}{\psi} \quad \text{for } \psi \ll 1, \quad (2.60)$$

which means that the last integral in (2.59) has a logarithmic divergence at the lower limit of integration. Therefore $\lambda = \infty$ in this case, as expected.

In the asymptotic limit $\psi \rightarrow 0$, it is possible to rewrite (2.56) as

$$\frac{d^2\psi}{dx^2} \simeq (1 - \mathcal{M}^{-2})\psi, \quad (2.61)$$

which gives

$$\psi(x) \simeq \psi_0 \exp\left[-x\sqrt{1 - \mathcal{M}^{-2}}\right], \quad (2.62)$$

for some unknown constant ψ_0 . This also shows that the wavelength is infinite, since $\mathcal{M} > 1$.

⁶Some might worry that λ_D in (2.38) does not have the proper physical dimension of *length* since the dimension of n_0 is *length inverse*, and not length inverse *cubed* as is usually the case in three dimensions. There is however not anything conceptually wrong with this definition, since the dimension of ϵ_0 can be said to be defined from (2.48), and thus already accounts for the dimensionality of n_0 .

2.3 Shockwaves

As has been pointed out in the previous section, the soliton is symmetric and therefore does not dissipate energy, unlike shockwaves. To get shock solutions, one has to break this symmetry. Reflected ions is one way of introducing asymmetry to the model [1, 2]. The reasoning behind the idea of ion reflection is that the rise in electrostatic potential, that is the wave, creates a potential barrier for the positively charged ions; so if an ion does not have enough kinetic energy to pass this potential barrier, it will be reflected back upstream. It is worth noting that introducing ion reflection to the model requires finite ion temperature. Otherwise the ion distribution would be concentrated to a single velocity, u , and the ions would either all be reflected or all pass through to the downstream region. Indeed, (2.44) in the soliton model guarantees that $Z_i e \phi_{\max} \leq m_i V^2/2$, meaning that no ions will be reflected. By introducing a finite ion temperature there will be a small number of reflected ions, breaking the symmetry between the up- and downstream.

This idea that the ion reflection creates the asymmetry of the shockwave was realized already in the 1960s [18, 19], and a semi-analytical kinetic model implementing this idea has been presented and studied by Cairns et al. [10, 11]. However the model by Cairns et al. treats the downstream ions in a slightly unsatisfying manner. This is addressed by Pusztai et al. [12] using a slightly different model for the downstream ions, which is then verified against a fully-kinetic Vlasov-Poisson simulation. In this section, the model used by Pusztai et al. is presented, and later extended to also account for trapped electrons.

As before, the electrostatic shockwave is described in the frame of the shock, i.e. with a bulk flow of incoming plasma from $x = +\infty$ with average velocity $-V$, and with the first potential maximum at $x = 0$. In this frame of reference the electrostatic potential, $\phi(x)$, is stationary and has the general form of rising from $\phi = 0$ at $x = +\infty$ to a maximum value, $\phi = \phi_{\max}$ at $x = 0$, and then oscillating at $x < 0$. See Figure 2.3 for a typical form of the electrostatic potential.

While the first few moments of the Vlasov equation for cold ions, (2.42) and (2.43), were sufficient to show the existence of solitons, the cold-ion approximation cannot be used here. Kinetic effects must be considered, hence the Vlasov equation has to be used instead of the fluid equations. For an ion distribution, f_j , the time-independent electrostatic Vlasov equation is

$$v \frac{\partial f_j}{\partial x} - \frac{e Z_j}{m_j} \frac{\partial \phi}{\partial x} \frac{\partial f_j}{\partial v} = 0, \quad (2.63)$$

which has the general solution $f_j = f_j(E_j)$, where $E_j = m_j v^2/2 + e Z_j \phi(x)$ is the total energy of an ion. The ions in the unperturbed ($\phi = 0$) plasma is assumed to follow a shifted Maxwellian distribution,

$$f_j(v) = \frac{n_{j,0}}{\sqrt{2\pi T_j/m_j}} \exp\left[-\frac{m_j(v+V)^2}{2T_j}\right]. \quad (2.64)$$

For the purposes of studying the shock, only the *incoming* ions are of interest, i.e. only $v \leq 0$ need to be considered. This is because in the steady state, any ion with $v > 0$

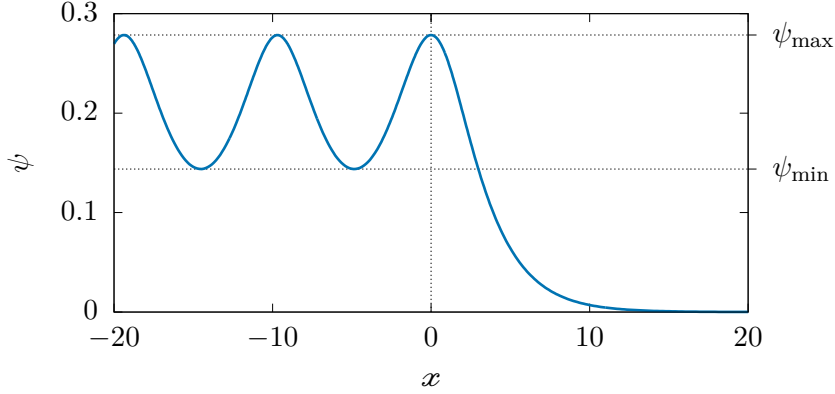


Figure 2.3: The normalized electrostatic potential, ψ , as a function of normalized position, x , for a fully ionized pure hydrogen plasma, with Maxwell-Boltzmann distributed electrons. The plasma is flowing in from the right with Mach number $\mathcal{M} = 1.15$ and electron-to-ion-temperature ratio $\tau_i \equiv Z_i T_e / T_i = 50$. The maximum value of the potential is $\psi_{\max} \approx 0.28$, and the downstream minimum value is $\psi_{\min} \approx 0.14$.

would have already left the shockwave behind. This is assuming that there is no supply of high energy ions coming from downstream, which is the case for collisionless shocks as are studied here. Under these conditions (2.64) can be written as

$$\begin{aligned} f_j &= \frac{n_{j,0}}{\sqrt{2\pi T_j/m_j}} \exp\left[-\frac{(|v| - V)^2}{2T_j/m_j}\right] \\ &= \frac{n_{j,0}}{\sqrt{2\pi T_j/m_j}} \exp\left[-\frac{m_j}{2T_j} \left(\sqrt{\frac{2E_j(v, \phi = 0)}{m_j}} - V\right)^2\right], \end{aligned} \quad (2.65)$$

which now is in the desired form $f_j = f_j(E_j)$. From here the distribution function is extended to finite values of ϕ (i.e. finite x) by using $E_j(v, \phi = 0) \rightarrow E_j(v, \phi)$, which yields

$$f_j(E_j(v, \phi)) = f_j(v, \phi) = \frac{n_{j,0}}{\sqrt{2\pi T_j/m_j}} \exp\left[-\frac{m_j}{2T_j} \left(\sqrt{v^2 + \frac{2eZ_j\phi}{m_j}} - V\right)^2\right]. \quad (2.66)$$

Introducing the dimensionless variables

$$\psi := \frac{e\phi}{T_e}, \quad u := \frac{v}{c_s} = \frac{v}{\sqrt{Z_i T_e/m_i}}, \quad \zeta_j := \frac{Z_j m_i}{m_j Z_i} \quad \text{and} \quad \tau_j := \frac{m_j c_s^2}{T_j} = \frac{Z_i T_e m_j}{T_j m_i}, \quad (2.67)$$

the ion distribution function can be written as

$$f_j = n_{j,0} \sqrt{\frac{\tau_j}{2\pi}} \exp\left[-\frac{\tau_j}{2} \left(\sqrt{u^2 + 2\zeta_j \psi} - \mathcal{M}\right)^2\right]. \quad (2.68)$$

The normalized densities and distribution functions are

$$\boldsymbol{n} := \frac{n}{n_0} \quad \text{and} \quad \boldsymbol{f} := \frac{f}{n_0/c_s} \quad (2.69)$$

respectively, where $n_0 := \sum_j Z_j n_{j,0}$.

Note that the normalization of position and density defines two separate length scales, λ_D and $1/n_0$ (the model is 1D). This is not a problem as long as the two length scales are kept separate, which they are in all the calculations here; except in the very end in Poisson's equation, where they are connected via ϵ_0 that unites the two different length scales. Nonetheless using two different length scales in a normalization could potentially cause problems if not handled properly, e.g. when going to higher dimensions. A similar problem arises with the normalizations of ϕ and T_j which both define different energy scales, that is however not a problem either.

The next step is to calculate the ion densities; as in (2.1) this is done by integrating the distribution function over all allowed velocities. From the above argument, the incoming ions were all assumed to have $\boldsymbol{v} \leq 0$. However, the full ion density also contains the reflected ions; these ions are the ones with $\mathcal{E}_j := \frac{1}{2}\boldsymbol{v}^2 + \zeta_j\psi < \zeta_j\psi_{\max}$, which means that their reflected (positive) velocity is

$$\boldsymbol{v} < \boldsymbol{v}_0(\psi) = \sqrt{2\zeta_j(\psi_{\max} - \psi)}. \quad (2.70)$$

Since these ions are reflected back upstream, they must be removed from the downstream distribution. In both [10] and [12], (2.68) is taken to hold for the reflected ions as well. This leads to the ion densities

$$\boldsymbol{n}_j^{(\text{us,ds})}(\psi(\boldsymbol{x})) = \int_{-\infty}^{\pm \boldsymbol{v}_0(\psi)} \boldsymbol{f}_j(\boldsymbol{v}, \psi) d\boldsymbol{v}, \quad (2.71)$$

where “us” and “ds” stands for up- and downstream respectively, and the integration limit $+\boldsymbol{v}_0(\psi)$ is for the upstream and $-\boldsymbol{v}_0(\psi)$ corresponds to the downstream density respectively. Unfortunately the integral in (2.71), with \boldsymbol{f}_j from (2.68), lacks a closed-form analytical expression for arbitrary ψ ; instead the integral has to be evaluated numerically. However, in the far upstream region, where $\psi = 0$ but the plasma is still affected by the shock through the reflected ions, the ion densities can be explicitly calculated as

$$\begin{aligned} \boldsymbol{n}_{j,1} = \boldsymbol{n}_j^{(\text{us})}(\psi = 0) &= \boldsymbol{n}_{j,0} \sqrt{\frac{\tau_j}{2\pi}} \int_{-\infty}^{\boldsymbol{v}_0(\psi=0)} \exp\left[-\frac{\tau_j}{2}(|\boldsymbol{v}| - \mathcal{M})^2\right] d\boldsymbol{v} \\ &= \frac{\boldsymbol{n}_{j,0}}{2} \left\{ 1 + 2 \operatorname{erf}\left[\sqrt{\frac{\tau_j}{2}} \mathcal{M}\right] + \operatorname{erf}\left[\sqrt{\frac{\tau_j}{2}} (\sqrt{2\zeta_j\psi_{\max}} - \mathcal{M})\right] \right\}, \end{aligned} \quad (2.72)$$

where “erf” is the usual error function

$$\operatorname{erf}(s) := \frac{2}{\sqrt{\pi}} \int_0^s e^{-s'^2} ds'. \quad (2.73)$$

Note that $n_{j,1} \neq n_{j,0}$; the former is the density far enough upstream that the potential has vanished but where the reflected ions are still present, whereas the latter is the ion density of the unperturbed *incoming* plasma.

The electron density, n_e , is also needed to calculate the electrostatic potential. Here, a few different models for the electron density can be used. In any case, the only reasonable dependencies that n_e can have are the electrostatic potential, ϕ , and the electron temperature, T_e . The only way to write down a functional dependence through these parameters is through the previously introduced dimensionless potential $\psi = e\phi/T_e$, which means that the normalized electron density

$$n_e = n_e(\psi) = n_{e,1}\eta(\psi), \quad (2.74)$$

where $\eta(\psi)$ is normalized so that $\eta \rightarrow 1$ as $\psi \rightarrow 0$. The constant $n_{e,1}$ is calculated from the quasi-neutrality condition in the far upstream region ($\psi \rightarrow 0$)

$$n_{e,1} = \sum_j Z_j n_{j,1}. \quad (2.75)$$

The simplest model for the electron distribution is a Maxwell-Boltzmann distribution, which leads to an electron density of

$$n_e^{(\text{MB})}(\psi) = n_{e,1} \exp(\psi). \quad (2.76)$$

This is what is used in [10–12].

The total normalized charge density is given by

$$\rho^{(\text{us,ds})}(\psi, \psi_{\text{max}}) = \sum_j Z_j \left[n_j^{(\text{us,ds})}(\psi, \psi_{\text{max}}) - n_{j,1}(\psi_{\text{max}})\eta(\psi) \right]. \quad (2.77)$$

Note that while Z_j is hidden under the normalized variables ζ_j and τ_j , it still appears here as just Z_j . This is because Z_j is a dimensionless quantity and cannot be normalized away completely. The normalized Poisson equation, with $x := x/\lambda_D$ as in (2.56), is given by

$$\frac{d^2\psi}{dx^2} = - \begin{cases} \rho^{(\text{us})}(\psi, \psi_{\text{max}}), & x \geq 0, \\ \rho^{(\text{ds})}(\psi, \psi_{\text{max}}), & x < 0. \end{cases} \quad (2.78)$$

Also note that ρ is continuous at $x = 0$, since $\psi = \psi_{\text{max}}$ there and $v_0(\psi_{\text{max}}) = 0$. Just as before, a Sagdeev potential is introduced,

$$\Psi_{\text{us}}(\psi, \psi_{\text{max}}) = \int_0^\psi d\psi' \rho_{\text{us}}(\psi', \psi_{\text{max}}). \quad (2.79)$$

The Sagdeev potential for the shock in Figure 2.3 is shown in Figure 2.4. So far, all presented quantities have had implicit dependencies on ψ_{max} , so there has been no easy way of calculating the value of ψ_{max} . That is, up until now. Recalling (2.58), it is clear

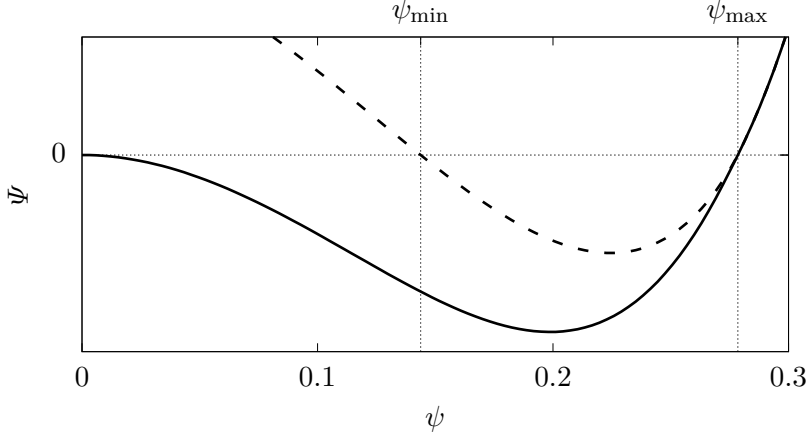


Figure 2.4: The up- and downstream Sagdeev potentials, solid and dashed lines respectively, for a shock with $\mathcal{M} = 1.15$ and $\tau_i = 50$. Note that the corresponding electrostatic potential, $\psi(x)$ which is shown in Figure 2.3, has precisely the same values of ψ_{\min} and ψ_{\max} as is given here.

that $d\psi/dx = 0$ requires $\Psi = 0$, but the derivative must also be zero at a *maximum* $\psi = \psi_{\max}$; therefore

$$\Psi_{\text{us}}(\psi = \psi_{\max}, \psi_{\max}) = \int_0^{\psi_{\max}} d\psi' \rho_{\text{us}}(\psi', \psi_{\max}) = 0. \quad (2.80)$$

This is the key equation of this whole chapter. By solving this equation, the rest of the electrostatic potential can easily be calculated numerically by solving (2.78).

For future reference, the downstream Sagdeev potential also has to follow (2.49) and satisfy $\Psi_{\text{ds}}(\psi = \psi_{\max}, \psi_{\max}) = 0$, which means that it has to be given by

$$\Psi_{\text{ds}}(\psi, \psi_{\max}) = \int_{\psi_{\max}}^{\psi} d\psi' \rho_{\text{ds}}(\psi', \psi_{\max}), \quad (2.81)$$

and is shown in Figure 2.4 in comparison with the upstream Sagdeev potential. The lower bound of the downstream electrostatic potential, is a *minimum*, where $d\psi/dx = 0$, so ψ_{\min} is of course given by

$$\Psi_{\text{ds}}(\psi = \psi_{\min}, \psi_{\max}) = \int_{\psi_{\max}}^{\psi_{\min}} d\psi' \rho_{\text{ds}}(\psi', \psi_{\max}) = 0. \quad (2.82)$$

In practice, both (2.82) and (2.80) have to be solved numerically since there is no analytical expression for $n_j(\psi)$ for an arbitrary value of ψ .

The shape of the electrostatic potential of the shock can now be understood within the mechanical analogy as a particle first gliding in the *upstream* Sagdeev potential from $\psi = 0$ to ψ_{\max} , and there the particle switches to the *downstream* Sagdeev potential where it will oscillate back and forth between ψ_{\min} and ψ_{\min} . This is illustrated when comparing the electrostatic potential in Figure 2.3 to its corresponding Sagdeev potentials in Figure 2.4, where ψ_{\min} and ψ_{\min} have been marked out and agrees precisely. The fact that ψ_{\max} is the same in both cases is not that remarkable since the numerical ODE solution was initiated using ψ_{\max} , however the value of ψ_{\min} is independently computed in the two different methods, and they agree up to the precision of the numerical solution schemes.

2.3.1 Trapped electrons

Returning to the electron distribution, there are many different ways to model the electrons. The simplest being the Maxwell-Boltzmann distribution, leading to the electron density in (2.76). However, a Maxwell-Boltzmann distribution assumes that the electrons are completely thermalized, i.e. that they have had enough time to dissipate any perturbations from a thermal background distribution. Shocks, on the other hand, are usually quite fast phenomena; in collisionless or low-collisionality shocks the electron thermalization timescale is much longer than the time it takes for the shock to pass. This would suggest that the Maxwell-Boltzmann distribution might not be the most accurate description for the electrons.

Among the strongest objections against the Maxwell-Boltzmann distribution in this scenario is the fact that the potential crests trap the electrons, which are negatively charged. This will affect the electron density and therefore also the potential. In a paper from 1968, Gurevich [20] calculates the distribution function of trapped particles in an adiabatically varying electrostatic field. The distribution function for trapped electrons found by Gurevich is flat in the trapping region of phase space while still being continuous on the boundary layer of the trapping region. The passing electrons follow their initial distribution functions, unaffected by the trapped electrons. Similar behavior has also been observed in simulations [12]. For an initially Maxwellian electron distribution, the trapped electron distribution function would therefore be

$$f_e^{(\text{tr})}(\phi \geq \phi_{\text{tr}}) = \frac{n_{e,1}}{\sqrt{2\pi T_e/m_e}} \exp\left(\frac{e\phi_{\text{tr}}}{T_e}\right), \quad (2.83)$$

inside the trapped electron region, where ϕ_{tr} is the potential at the boundary of the trapping region, above which the electrons are trapped. This then leads to a normalized electron density of

$$n_e^{(\text{tr})} = n_{e,1} \left[\frac{2}{\sqrt{\pi}} \sqrt{\psi - \psi_{\text{tr}}} \exp(\psi_{\text{tr}}) + \exp(\psi) \operatorname{erfc}\left(\sqrt{\psi - \psi_{\text{tr}}}\right) \right], \quad (2.84)$$

where “erfc” is the complementary error function, defined as

$$\operatorname{erfc}(s) := \frac{2}{\sqrt{\pi}} \int_s^\infty e^{-s'^2} ds' = 1 - \operatorname{erf}(s). \quad (2.85)$$

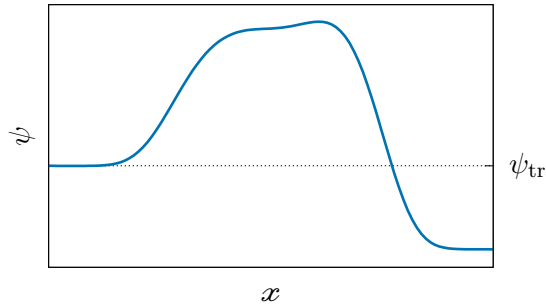


Figure 2.5: An example potential illustrating the trapping level ψ_{tr} . The trapping level is the higher value of the potential at either end point of the trapping region. The trapping is independent of the shape of the potential inside the trapping region.

Note that $n_e^{(\text{tr})} \rightarrow n_e^{(\text{MB})}$ when $\psi \rightarrow \psi_{\text{tr}}$, as is expected.

That the field is adiabatically varying means that the field evolves smoothly and much slower than the electron motion. In the case of the shocks here, the time it takes for the shock to pass over a length L is $t_{\text{shock}} = L/V \sim L/c_s \sim L/\sqrt{T_e/m_i}$, while for electrons the same length is passed in roughly $t_e \sim L/v_e \sim L/\sqrt{T_e/m_e}$, or in other words

$$\frac{t_{\text{shock}}}{t_e} \sim \sqrt{\frac{m_i}{m_e}} \gg 1. \quad (2.86)$$

That is, the electrons are much faster than the shock, which means that it is safe to say that the shock potential is varying adiabatically.

The trapping level ψ_{tr} in (2.84), above which the electrons get trapped, is given as the higher of the two bounding values of the trapping region, as is illustrated in Figure 2.5. It should also be pointed out that the trapping is independent of the shape of ψ inside the trapping region, i.e. (2.84) holds for any $\psi > \psi_{\text{tr}}$ inside the trapping region. With this in mind it is natural to take $\psi_{\text{tr}} = \psi_{\text{min}}$, making each hump in the downstream electrostatic potential a trapping region. This model is called the *adiabatic trapping* (AD) model in this thesis. Practically, this means that (2.80) and (2.82) have to be solved (numerically) simultaneously as a system of equations with two unknowns and two independent equations.

However, simulation results [12] have also indicated that setting $\psi_{\text{tr}} = \psi_{\text{min}}$ is not exactly right. Also, while in this theoretical model of the shock the downstream oscillations are indefinite, in a real shockwave the potential oscillations will eventually decay down in the far down stream region; other limitations, like the physical size of the plasma, will also prevent indefinite downstream oscillations. In that case, a situation resembling the one in Figure 2.5 might arise, where the potential at the back end is higher than in the front. It is therefore also interesting to study a model where ψ_{tr} varies more freely, like for instance $\psi_{\text{tr}} = C_{\text{tr}}\psi_{\text{max}}$. Note that a value of the trapping coefficient of $C_{\text{tr}} = 1$ corresponds to fully free Maxwell-Boltzmann electrons, and at points where $C_{\text{tr}} = \psi_{\text{min}}/\psi_{\text{max}}$ the AD model is recovered.

Chapter 3

Effects of electron trapping on collisionless shocks

To study the behavior of the different shock models some form of numerical method must be employed. This is because the integral defining the ion density, (2.71), lacks a closed analytical form. In this chapter, a short account of how the different shock models were implemented numerically is presented, along with some results obtained from the trapped electron models.

3.1 Numerical implementation

For finding the behavior of the shocks in the models from section 2.3, a series of *Matlab* classes have been implemented. In this section, a brief overview of how this has been done is presented.

The different shock classes create “shock objects”, which are initialized with the input parameters \mathcal{M} , T_e/T_i , m_j/m_p , Z_j , and $n_{j,0}$. The class then calculates ψ_{\max} and ψ_{\min} , as well as other model specific parameters, using the Sagdeev potential method, (2.80) and (2.82).

These Matlab classes are open source and available on GitHub¹. Do however note that the normalization used in the code, at the time of writing, is not the same as in the thesis; to convert to this normalization use $\psi = \text{phi}/\text{tau}$ and $x = \mathbf{x}/\text{sqrt}(\text{tau})$, where $\text{tau} := T_e/T_i$. There are plans to change the normalization of the code. When the normalization has been changed, it will be announced in the GitHub repository.

Initializing a shock object

As was said when the Sagdeev potential method was introduced to the shock model, many of the other quantities have some form of implicit dependence on either ψ_{\max} , ψ_{\min} or both, and it was first with the Sagdeev potential that a method for finding ψ_{\max} or ψ_{\min}

¹https://github.com/andsunds/Shock_pkg

was presented. As such, the numerical implementation relies on solving (2.80) and (2.82) numerically using a bisection method. This is done by guessing some initial $\tilde{\psi}_{\max}$ and then numerically integrating $\rho_{\text{us}}(\psi', \tilde{\psi}_{\max})$, which in turn consists of a numerical integration to calculate $n_j^{(\text{us})}$ according to (2.71) for each ψ' . This procedure is then repeated for a different $\tilde{\psi}_{\max}$ in a numerical root finder until the final integral in (2.80) is sufficiently close to zero. The numerical precision is set by another input parameter, `tol`, which determines the tolerances in each numerical step; in the numerical integration `tol` is the tolerance in the relative error, while when finding roots `tol` is set as the tolerance in the absolute function value. All runs in this thesis have been done at `tol` = 10^{-6} or better.

In the AD trapped electron model, where the electron trapping level is set at $\psi_{\text{tr}} = \psi_{\text{min}}$. The electron density also depends on ψ_{min} , which results in the system of equations

$$\begin{cases} \Psi_{\text{us}}(\psi = \psi_{\max}, \psi_{\max}, \psi_{\min}) = 0 \\ \Psi_{\text{ds}}(\psi = \psi_{\min}, \psi_{\max}, \psi_{\min}) = 0. \end{cases} \quad (3.1)$$

The procedure for finding the roots here is similar, but due to the higher dimensionality some least square method has to be used instead – e.g. a trust region or a Levenberg–Marquardt algorithm.

Some times, depending on the initial guess of ψ_{\max} , the numerical algorithms above find unphysical roots. These roots correspond to a potential minimum, and an unbounded $\psi(x)$, which are clearly unphysical. To avoid any of these roots, the charge density at $\psi = \psi_{\max}$ is calculated, and checked so that

$$\left. \frac{d^2\psi}{dx^2} \right|_{x=0} = -\rho_{\text{us}}(\psi_{\max}, \psi_{\max}) = -\rho_{\text{ds}}(\psi_{\max}, \psi_{\max}) < 0. \quad (3.2)$$

This corresponds to an actual *maximum* of ψ at $x = 0$. If this check is not satisfied, the values of ψ_{\max} and ψ_{\min} are set to NaN and the shock object is discarded.

Although this method involves evaluating two nested numerical integrations several times, runtimes are very fast compared to PIC (particle in cell) or Vlasov solvers. The computational time required to find ψ_{\max} and ψ_{\min} ranges from a couple of seconds up to at most a few minutes depending on the input parameters and how good the initial guess is. Although the upper limit is a few minutes, the absolute majority of runs take around 10s. These runtimes are on a single core in a medium to high performance workstation PC. Methods like PIC or Vlasov solvers generally have considerably longer runtimes, running on large clusters. However that is heavily dependent on the size of the problem; this problem which only involves one spatial and one velocity dimension is not very heavy. Nonetheless having a semi-analytical model significantly reduces the computational resources required.

Using the shock objects

Once ψ_{\max} and ψ_{\min} have been found, they can then be used to calculate other quantities of interest. Perhaps the most common quantity to one would want to calculate is $\psi(x)$,

which is calculated by numerically solving (2.78) with the initial conditions

$$\psi(x=0) = \psi_{\max} \quad \text{and} \quad \left. \frac{d\psi}{dx} \right|_{x=0} = 0, \quad (3.3)$$

using some Runge-Kutta method – the problem is not stiff. When finding $\psi(x)$, the user also has the options to get $E(x) = -\partial\psi/\partial x$ and $\rho(x) = -\partial^2\psi/\partial x^2$ at the same time.

There is also a function for calculating $\Psi_{\text{us,ds}}(\psi)$, used mostly for checking the solutions together with $\psi(x)$, confirming that the found ψ_{\min} and ψ_{\max} are correct – like in Figure 2.3 and Figure 2.4. Although not shown in any figure in this thesis, a function calculating the wavelength of the downstream potential oscillation, from (A.5) in Appendix A, has also been implemented. This function has also been used to check the solution, $\psi(x)$.

As was mentioned before, the runtime and risk of finding unphysical solutions depends on the initial guess of ψ_{\max} . Therefore when doing scans in some parameter, most notably the Mach number, a function for stepping through a range of parameter values have been implemented. The function, for e.g. Mach numbers, takes in a precalculated shock object at some Mach number in the middle of the range, and then takes small steps in either direction, using the $\psi_{\max,\min}$ of each previous step as the initial guess of the next step. This function, and similar other functions, have been used to produce the various different scans presented in the following section.

Lastly, it should be pointed out that the previous studies of this model [10–12] have used a different normalization. Whereas the normalization in this thesis is based on c_s and, ultimately, the electron temperature T_e , the previous normalizations have been based on the ion temperature. This means that results will not be directly comparable in terms of the numerical values obtained from the models, even though the models are essentially the same. The conversion factors to get from this normalization to the one in [12] are T_e/T_i for the electrostatic potential and $\sqrt{T_e/T_i}$ for the position.

3.2 Numerical results

As the behavior of free electron shocks have already been studied elsewhere [10–12], the numerical studies of this thesis will mostly focus on the effects of the electron trapping. One benefit of using a properly chosen normalization is that it reduces the number unknowns through the Buckingham Π -theorem [21]. Furthermore only single-ion-species plasmas will be considered here; effects of small impurities have been studied in [12]. This means that the parameter $\zeta_j \rightarrow \zeta_i \equiv 1$ is fixed, and only the effects of τ_i , \mathcal{M} , and C_{tr} , will have to be studied. This will be done through a series of scans over primarily the Mach number, \mathcal{M} , but also over the trapping coefficient, C_{tr} . Scans have also been performed at different τ_i .

Note that Z_i will still appear in the expression for the charge density, (2.77), even in a single ion species plasma. However the normalization of density results in

$$n_{i,0} = \frac{n_{i,0}}{n_0} = \frac{1}{Z_i} \quad (3.4)$$

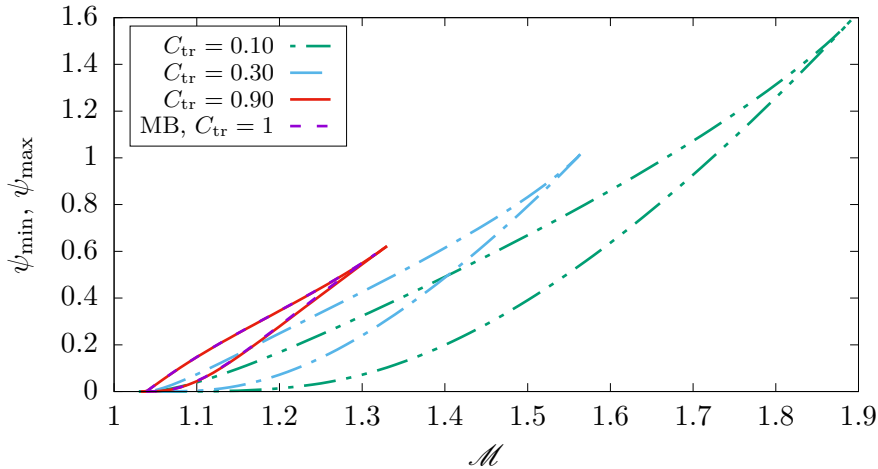


Figure 3.1: The values of ψ_{\max} and ψ_{\min} in the trapped electron model for some different values of the trapping coefficients, C_{tr} , with $\tau_i = 40$. The range of solutions is significantly larger for the rather low values of $C_{\text{tr}} = 0.10$ and 0.30 .

for a single ion species plasma. This, together with the fact that all other relevant densities are proportional to $n_{i,0}$, means that (2.77) is in fact independent of Z_i . For a multi-species plasma, however, this is no longer the case, and Z_j will still have to be considered together with the other parameters which have been normalized away for a single ion species plasma.

Beginning with scans over \mathcal{M} , which have been done with the electron trapping model, that had a freely set trapping level, for a few different values of the trapping coefficient C_{tr} at $\tau_i = 40$; this is to see how the shocks are affected by C_{tr} . The results from these scans are shown in Figure 3.1. The range of possible $\psi_{\min, \max}$ and the range of \mathcal{M} for which there exists a solution greatly increases for lower values of C_{tr} , i.e. larger trapping region. However for the same Mach number, decreasing C_{tr} yields a lower value of ψ_{\max} and ψ_{\min} . Even though the increased solution range can be quite large, it only becomes significant at very low values of C_{tr} . As Figure 3.1 shows, the difference between $C_{\text{tr}} = 0.90$ and the pure Maxwell-Boltzmann model ($C_{\text{tr}} = 1$) is extremely small. The treatment of ion reflection in Appendix A shows that the important parameter for ion reflection is $F_i := 2\psi_{\max}/\mathcal{M}^2$. So, although not shown here, the considerably increased range of ψ_{\max} in Figure 3.1 only slightly increases the maximum F_i for lower C_{tr} , due to the also increased range of \mathcal{M} . However the number of reflected ions is exponentially sensitive to F_i , so the trapping here still affects the ion reflection considerably.

The actual trapping level, $\psi_{\text{tr}} = C_{\text{tr}}\psi_{\max}$, is not shown in Figure 3.1, but it is still clear that at some Mach number $\psi_{\min} = \psi_{\text{tr}}$ since ψ_{tr} is constant and ψ_{\min} varies from 0 to ψ_{\max} . At these points, where $\psi_{\min} = \psi_{\text{tr}}$, the AD model is recovered, where each potential hump is its own trapping region. Therefore to further study this model, scans over C_{tr} were performed for some values of \mathcal{M} at $\tau_i = 40$. In Figure 3.2, ψ_{\min}/ψ_{\max} is compared to $\psi_{\text{tr}}/\psi_{\max} = C_{\text{tr}}$. There it is seen that the ψ_{\min}/ψ_{\max} curve only crosses the

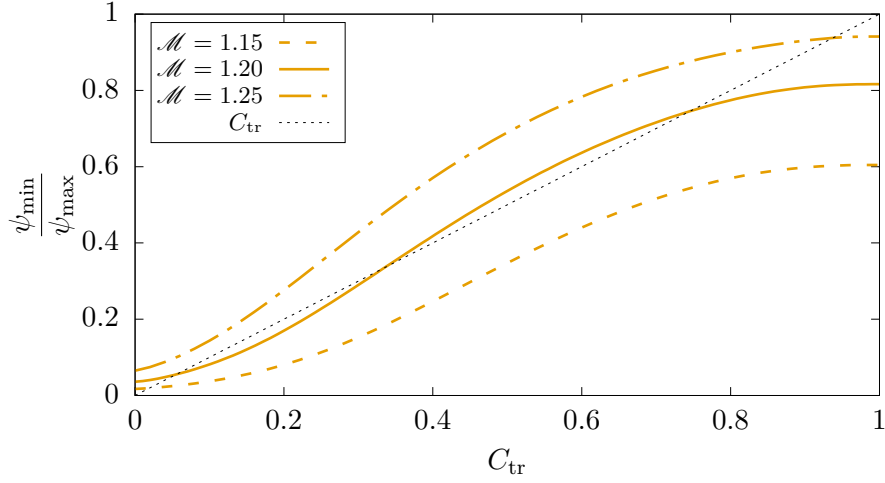


Figure 3.2: Comparison of ψ_{\min}/ψ_{\max} to $\psi_{\text{tr}}/\psi_{\max} = C_{\text{tr}}$ for three different values of \mathcal{M} . All three cases have $\tau_1 = 40$. Each point where the curves cross the line C_{tr} corresponds to the AD trapping model, where $\psi_{\min} = \psi_{\text{tr}}$. For $\mathcal{M} = 1.20$ there are three such crossings, while the others only have one each.

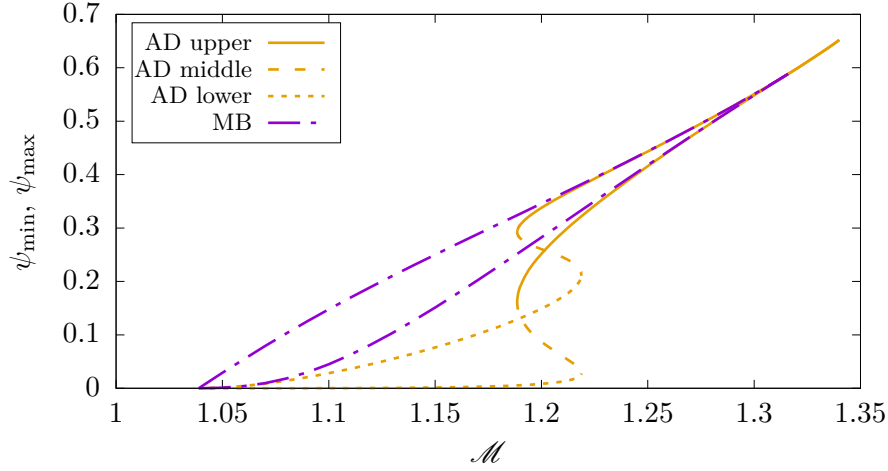


Figure 3.3: The values of ψ_{\max} and ψ_{\min} for shocks calculated using either the Maxwell-Boltzmann electron distribution (MB) or with adiabatically trapped electron model (AD), at an electron temperature of $\tau_1 = 40$. For Mach numbers above around 1.25, the AD model behaves similarly to the MB model. At lower \mathcal{M} however, the two models start to diverge; then in a region $\mathcal{M} \approx 1.19$ – 1.22 , there are three solutions in the AD model. Then below that, there is only one solution again which is considerably lower than the MB solution.

C_{tr} curve at one point each for $\mathcal{M} = 1.15$ and $\mathcal{M} = 1.25$, while for $\mathcal{M} = 1.20$ there are *three* different crossings. This means that there should be a region around $\mathcal{M} = 1.20$ where the AD model has three distinct solutions. This is confirmed in Figure 3.3, where the AD solutions are compared to the corresponding MB solution in a scan over \mathcal{M} , and there are indeed three AD solutions in a range $\mathcal{M} \approx 1.19\text{--}1.22$. For Mach numbers above this region of multiple solutions, the AD model rapidly approaches the MB model.

The form of the electrostatic potentials of the three different AD solutions (“upper”, “middle”, and “lower”) at $\mathcal{M} = 1.20$ and $\tau_i = 40$, together with the MB solution, are shown in Figure 3.4. In addition to the varying ψ_{min} and ψ_{max} , the wavelengths of the downstream oscillations differ by a factor 1.5–2 between each solution. In the upstream region on the other hand the decay is exponential² and fairly similar. Of course being able to initiate a shock with the highest ψ_{max} for the same \mathcal{M} and τ_i is desirable for achieving the most ions reflected.

The next step in the study of the AD model is to consider how τ_i affects the solutions. When decreasing τ_i the region of multiple solutions shrinks until it, somewhere between $\tau_i = 25$ and $\tau_i = 30$, vanishes. Then, for even lower τ_i , there is only one single solution for each Mach number. This is shown in Figure 3.5. When τ_i is increased the region of multiple solutions continues to grow as well as the total range of solutions, which is shown in Figure 3.6. Another effect of τ_i , most clearly seen in Figure 3.6, is that for the same Mach number ψ_{max} has increased. In the case

One final comment is that, as can be seen in Figures 3.1, 3.3, and 3.5, all Mach number scans start slightly above $\mathcal{M} = 1$. In fact most scans start at around $\mathcal{M} = 1.04\text{--}1.05$. This might be a bit unexpected since \mathcal{M} is usually defined so that $\mathcal{M} = 1$ constitutes the lower limit for which shocks exist, indeed the Mach number used in this thesis was defined based on the lower speed limit for the solitons in section 2.2. This Mach number was found to be based on the ion-acoustic wave propagation speed, c_s from (2.40). However since the shocks have finite ion temperature, (2.41) should be used instead. In this normalization (2.41) reads

$$u_{\text{phase}} = c_s \sqrt{1 + \frac{\gamma_i}{\tau_i}}, \quad (3.5)$$

and in 1D $\gamma_i = 3$; so for e.g. $\tau_i = 40$, $u_{\text{phase}} \approx 1.04c_s$ which is very close to the observed lower Mach number limit in Figure 3.3. The sentiment that shocks only form at or above the propagation speed of the linear waves, therefore continues to hold here. There might however exist higher order effects of the ion temperature, at even lower values of τ_i . For instance [11] describes a lower limit on T_e/T_i for the existence of shocks, but that is beyond the scope of this thesis.

²It is not clear from Figure 3.4 that the upstream decay is exponential, but it becomes obvious when the same curves are plotted using a log scale (not shown here).

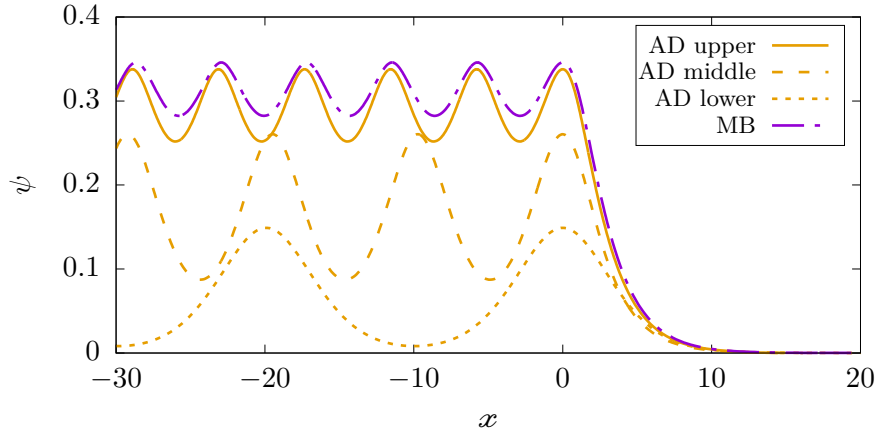


Figure 3.4: Electrostatic potentials calculated with either Maxwell-Boltzmann distributed electrons (MB) or adiabatically trapped electrons (AD), at Mach number $\mathcal{M} = 1.20$ and electron temperature $\tau_i = 40$. As can be seen in Figure 3.3, the AD model has three solutions at $\mathcal{M} = 1.20$ there, the forms of which are shown in this figure.

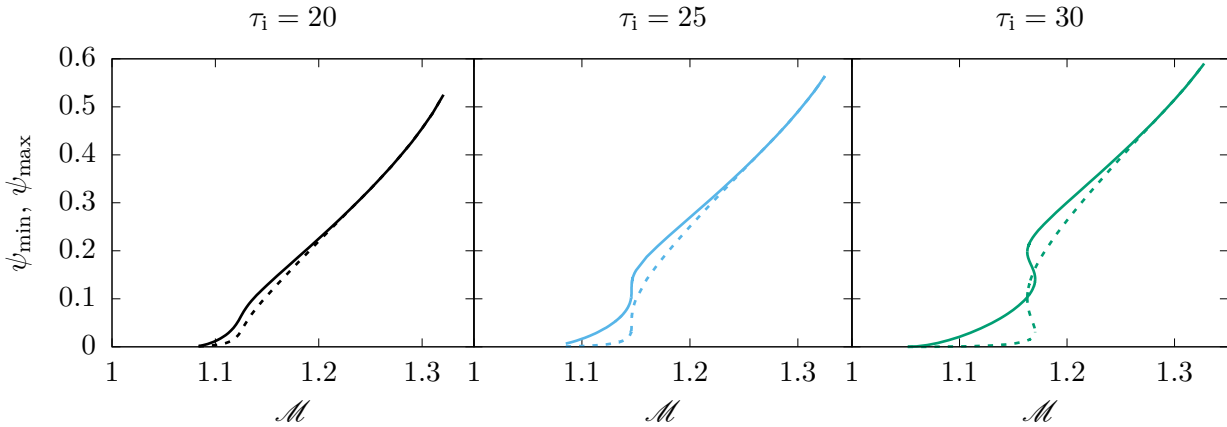


Figure 3.5: The values of ψ_{\min} and ψ_{\max} from the AD model as functions of Mach number, \mathcal{M} , for three different electron temperatures τ_i . The solutions are single-valued for $\tau_i = 20$ and 25, while for $\tau_i = 30$ the curves have just started to develop a region of multiple solutions.

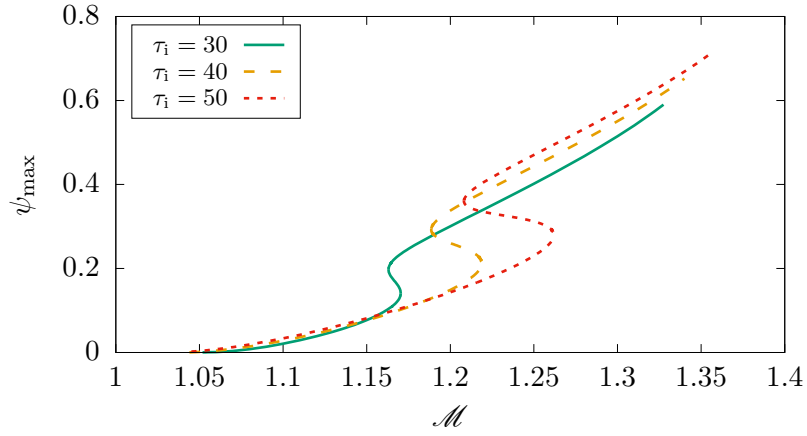


Figure 3.6: The values of ψ_{\max} in a single ion species plasma for different Mach numbers, \mathcal{M} , at different electron temperatures, τ_i , calculated with adiabatically trapped electrons (AD model).

Chapter 4

Weakly collisional shocks

In the shock models presented in section 2.3, any effects of binary collisions have so far been neglected. This is safe to do in hot, low-density plasmas where the particles virtually never collide with each other, as in for instance non-stellar space plasmas. However, in laboratory plasmas the densities can be much higher, and in such cases binary collisions may have to be considered. This chapter develops a theory for describing the effects of introducing a weak, but finite, collisionality in a time dependent, semi-analytical shock model.

4.1 Collisions and collision operators

Binary collisions happen on a particle-to-particle basis. It is therefore not immediately obvious how to handle them theoretically. This section will therefore take some time to go through the basics of how collisions are treated in kinetic theory. For a further study of collisional effects, the reader is referred to for instance the book by Helander and Sigmar [22].

The way collisions are studied in kinetic theory is through so called collision operators, $C[f]$. From a statistical mechanics viewpoint the distribution function does not represent each single individual particle, but rather a collective or statistical behavior of the particles. Similarly the collision operators cannot represent each single collision, instead they aim to capture how the collisions affect the distribution function. Therefore the collision operators are put in as a modification to the Vlasov equation, or in this case the electrostatic Vlasov equation

$$\frac{\partial f_a}{\partial t} + \mathbf{v} \cdot \frac{\partial f_a}{\partial \mathbf{x}} - \frac{Z_a e}{m_a} \frac{\partial \phi}{\partial \mathbf{x}} \cdot \frac{\partial f_a}{\partial \mathbf{v}} = C[f_a], \quad (4.1)$$

which in the context of collisions is just called the *kinetic equation*. The introduction of $C[f]$ to the RHS of the Vlasov equation makes sense in terms of the reasoning around phase space trajectories in section 2.1.2. Everything on the LHS corresponds to the phase space trajectory of a particle due to the macroscopic fields, but then the collisions will knock some particles off that trajectory resulting in f varying along the phase space trajectory, i.e. $C[f]$ instead of zero on the RHS.

The form and motivation of each collision operator differ from problem to problem. However, for problems dominated by binary collisions which only cause a small change in the momentum of the particles, the general collision operator is the *Fokker-Planck operator*, which using tensor index notation is

$$C_{ab}^{\text{FP}}[f_a, f_b] = \frac{\partial}{\partial v_i} \left[A_i^{(ab)} f_a + \frac{\partial}{\partial v_j} (D_{ij}^{(ab)} f_a) \right], \quad (4.2)$$

where $A^{(ab)}$ and $D^{(ab)}$ are functionals of f_b . The exact form of these functionals are not given here, but can be found in [22, Ch. 3.1]. The functional $A^{(ab)}$ is related to the average net force on species a due to collisions with species b , and $D^{(ab)}$ is the diffusion tensor of species a due to collisions with species b – the diffusion being in *velocity* space. Both $A^{(ab)}$ and $D^{(ab)}$ depend on \mathbf{v} .

4.1.1 Model collision operator for electrostatic shocks

As a first model, and to limit the scope of this thesis, only single ion species plasmas are considered. Furthermore, electron-ion collisions are neglected, and only one-dimensional configurations are considered. This means that the collision operator can be simplified somewhat.

The first major idea is to utilize the fact that the downstream ion distribution function, $f := f_i$, is discontinuous at the separatrix $v = -v_0$. Indeed, this is also a key motivation for studying the effects of collisions on shocks. This means that when introducing collisions, there will be a very thin boundary layer, around $v = -v_0$, across which f varies more sharply than anywhere else. Take $\delta v \ll v$ to be the characteristic width of that boundary layer. Then $\partial f / \partial v \sim f / \delta v$ and $\partial^2 f / \partial v^2 \sim f / \delta v^2$, which would mean that the dominant term in the Fokker-Planck operator is

$$C^{\text{FP}} \approx D \frac{\partial^2 f}{\partial v^2} \gg A \frac{\partial f}{\partial v}, \frac{\partial D}{\partial v} \frac{\partial f}{\partial v}, \text{ etc.} \quad (4.3)$$

In this context, and the rest of this thesis, the symbol “ \sim ” will be used to denote order of magnitude estimates.

Now, as was mentioned above, D is, in general, velocity dependent. Its derivative was neglected since the term with the second derivative of f dominates over all other terms. However for the purpose of creating a first collisional model, D is here assumed constant. Formally, for this to be valid the width of the trapped region has to be much smaller than the velocity of the ions in the middle of the distribution – i.e. $v_0 \ll \sqrt{\mathcal{M}^2 - 2\psi}$, which is equivalent to $2\psi_{\text{max}} / \mathcal{M}^2 \ll 1$. This condition is in general not satisfied for the shocks studied so far, and indeed those that will be studied in the rest of this thesis either. However if this condition would be satisfied the number of particles near the separatrix would be very small, and then collisional effects would be negligible. Also, as mentioned, this is supposed to be a first model for collisions, and as such this formal requirement will be neglected in the rest of this thesis. Keeping the velocity dependence would lead

to more complicated calculations of orbit-time-averages, but would likely not affect the results very much.

Based on the normalizations of position, λ_D , and speed, c_s , used previously, it is only natural to now introduce the normalized time

$$\mathfrak{t} = \frac{t}{\lambda_D/c_s}. \quad (4.4)$$

This elegantly normalizes (4.1) into

$$\frac{\partial \mathcal{f}}{\partial \mathfrak{t}} + \mathfrak{v} \frac{\partial \mathcal{f}}{\partial \mathfrak{x}} - \frac{\partial \psi}{\partial \mathfrak{x}} \frac{\partial \mathcal{f}}{\partial \mathfrak{v}} = \nu_* \frac{\partial^2 \mathcal{f}}{\partial \mathfrak{v}^2}. \quad (4.5)$$

Here the normalized *collisionality*

$$\nu_* := \frac{\lambda_D D}{c_s^3} \ll 1 \quad (4.6)$$

has also been introduced based on the physical dimension of D . This is also the small collision parameter referred to when speaking of a “weak collisionality” in this thesis.

4.2 Introducing a small collisionality

The previous shock model in section 2.3 was static, $\partial f/\partial t = 0$, and collisionless, $\nu_* = 0$. It is therefore natural to try and extend the model using a weak, but finite, collisionality $\nu_* \ll 1$. This section presents the derivation of the time dependent, semi-analytical model that accounts for weak ion collisions.

When the collisionality $\nu_* \ll 1$ is introduced, the time dependence of \mathcal{f} is assumed to only stem from collisions. Therefore $\partial \mathcal{f}/\partial \mathfrak{t}$ is assumed to be of the same order of magnitude as ν_* . When having these small perturbations to the system it is customary to try to find a solution in the form of a perturbation expansion,

$$\mathcal{f} = \mathcal{f}_0(\mathfrak{t}, \mathfrak{x}, \mathfrak{v}) + \mathcal{f}_1(\mathfrak{t}, \mathfrak{x}, \mathfrak{v}) + \dots, \quad \text{with } \mathcal{f}_1 \sim \nu_* \mathcal{f}_0 \ll \mathcal{f}_0. \quad (4.7)$$

Using this ordering, the lowest order perturbation equation obtained from (4.5) is

$$\mathfrak{v} \frac{\partial \mathcal{f}_0}{\partial \mathfrak{x}} - \frac{\partial \psi}{\partial \mathfrak{x}} \frac{\partial \mathcal{f}_0}{\partial \mathfrak{v}} = 0, \quad (4.8)$$

which is just the original equation of the collisionless shock model, (2.63). This means that $\mathcal{f}_0(\mathfrak{t}, \mathfrak{x}, \mathfrak{v}) = \mathcal{f}_0(\mathfrak{t}, \mathcal{E})$, with $\mathcal{E} = \mathfrak{x}^2/2 + \psi$.

The shocks are also assumed to form on short enough time scales, compared to the collisionality ν_* , so that the collisionless shock model can be used as the initial condition for these weakly collisional shocks. As such, the electrostatic potential in the downstream region is assumed to be periodic and semi-infinite. In phase space this corresponds to a periodic and semi-infinite chain of linked “islands of trapping”, marked as region II in Figure 4.1. This periodicity will be used later on. In reality, the downstream oscillations

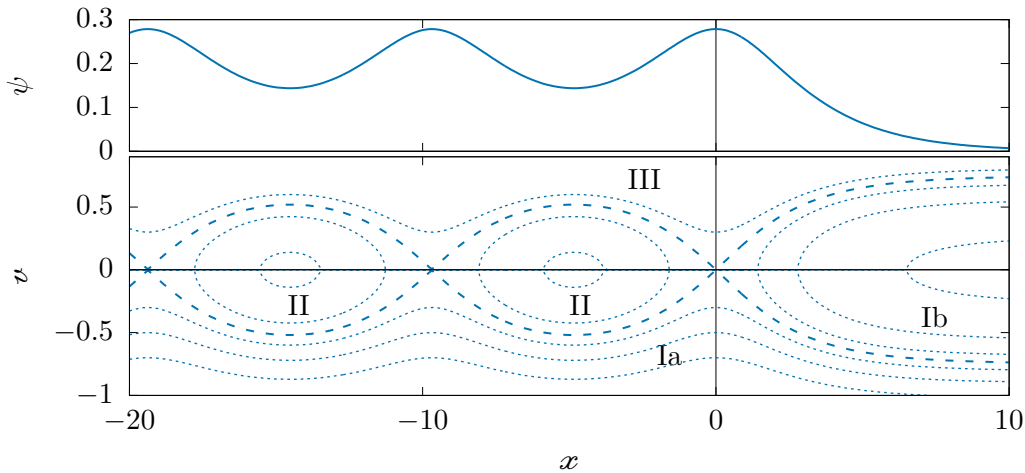


Figure 4.1: The same shock as in Figure 2.3, together with a phase space plot showing constant energy contours (dotted lines), and the separatrices (dashed lines) between regions I, II, and III, corresponding to $v = \pm v_0 = \pm\sqrt{2(\psi_{\max} - \psi)}$. Ions inside an “island” of region II will orbit around along their closed constant energy contour, and are therefore trapped. Region III contains the co-passing ions, which move forward and pass the shock, and lastly region Ia and Ib have the passing and reflected ions respectively.

cannot extend indefinitely, and there will be effects which dampen the amplitude of the oscillations making them non-periodic. For the purposes of studying the shockwave, most interest is focused to the vicinity of the shock front and how it is affected by the collisions; the downstream potential oscillations can therefore very well be approximated as periodic and semi-infinite.

Looking at the phase space plot in Figure 4.1, there are four regions marked out and they are separated by two separatrices. In the original, collisionless, shock model only regions Ia and Ib are populated. The ions in region Ib are the ones that do not have enough energy to make it over the potential barrier of the shock front and will thus get reflected back upstream. The ions in region Ia on the other hand, have enough energy to pass the shock front down into the downstream region. The collisionless model would therefore have a sharp discontinuity in the ion distribution function at the separatrices between regions Ia and II, and between Ib and III. This discontinuity is what is hoped to be remedied by introducing a small collisionality. The collisions would act to diffuse ions in velocity space across the separatrices, and thus populating regions II and III with a small number ions in a very thin boundary layer near the separatrices.

4.2.1 Perturbative solution with orbit-time-averaging

The lowest order perturbation equation, (4.8), did not contain any collisions or time dependence. In the next order perturbation equation,

$$\frac{\partial f_0}{\partial t} + v \frac{\partial f_1}{\partial x} - \frac{\partial \psi}{\partial x} \frac{\partial f_1}{\partial v} = \nu_* \frac{\partial^2 f_0}{\partial v^2}, \quad (4.9)$$

both the collisionality and a time dependence of f_0 are introduced, however so is f_1 and the system is not closed.

In order to close the system an “orbit-time-average” is introduced,

$$\langle g \rangle_{\mathcal{E}} := \left[\oint_{\mathcal{E}} d\vartheta \right]^{-1} \oint_{\mathcal{E}} g d\vartheta \quad (4.10)$$

where

$$d\vartheta = \frac{dx}{v} \Big|_{\mathcal{E}} \quad (4.11)$$

represents a time coordinate along a *constant energy*, \mathcal{E} , contour. For particles in the trapped region, the constant energy contours are closed and the name “orbit time” is justified. However in regions I and III the contours are open, but as was mentioned above, the potential oscillation is assumed to be *periodic in the downstream region* ($x \leq 0$), so the integrations in (4.10) can be taken over one such period – e.g. from $x = -\lambda$ to $x = 0$ where λ is the wavelength of the downstream oscillation. Note that the orbit time coordinate, ϑ , is thought of as a time coordinate independent of t . The integrations are therefore performed keeping both \mathcal{E} and t fixed. This means that

$$\left\langle \frac{\partial}{\partial t} \right\rangle_{\mathcal{E}} = \frac{\partial}{\partial t}. \quad (4.12)$$

Another way of seeing this is to say that the orbits happen on time scales *much* faster than any collisional effects, meaning that any t dependence is negligible during the time span of the orbit integrals.

The next thing to note with the orbit-time-average is that

$$\left\langle v \frac{\partial g}{\partial x} - \frac{\partial \psi}{\partial x} \frac{\partial g}{\partial v} \right\rangle_{\mathcal{E}} = 0. \quad (4.13)$$

This is because the averaging is done over a constant energy, $\mathcal{E} = v^2/2 + \psi$, contour, and on this curve

$$0 = \frac{d\mathcal{E}}{d\vartheta} = v \frac{dv}{d\vartheta} + \frac{d\psi}{d\vartheta} = v \frac{dv}{d\vartheta} + \frac{\partial \psi}{\partial x} \Big|_{\mathcal{E}} \frac{dx}{d\vartheta}. \quad (4.14)$$

This means that

$$\frac{dg}{d\vartheta} = \frac{\partial g}{\partial x} \frac{dx}{d\vartheta} + \frac{\partial g}{\partial v} \frac{dv}{d\vartheta} = \frac{1}{v} \frac{dx}{d\vartheta} \left[v \frac{\partial g}{\partial x} - \frac{\partial \psi}{\partial x} \frac{\partial g}{\partial v} \right]_{\mathcal{E}} = \left[v \frac{\partial g}{\partial x} - \frac{\partial \psi}{\partial x} \frac{\partial g}{\partial v} \right]_{\mathcal{E}}, \quad (4.15)$$

that is

$$\left\langle v \frac{\partial g}{\partial x} - \frac{\partial \psi}{\partial x} \frac{\partial g}{\partial v} \right\rangle_{\mathcal{E}} = \left[\oint_{\mathcal{E}} d\vartheta \right]^{-1} \oint_{\mathcal{E}} \frac{dg}{d\vartheta} d\vartheta = 0 \quad (4.16)$$

where the last equality is assuming either that g is single valued in region II, or that g is periodic in regions I or III. Also note that $f_0 = f_0(t, \mathcal{E})$ only depends on the time t and energy, which means that

$$\langle f_0 \rangle_{\mathcal{E}} = f_0 \quad (4.17)$$

since the orbit-time-averages are performed at constant energy.

Now, applying the orbit-time-averaging to both sides of (4.9) yields

$$\frac{\partial f_0}{\partial t} = \nu_* \left\langle \frac{\partial^2 f_0}{\partial u^2} \right\rangle_{\mathcal{E}}, \quad (4.18)$$

which managed to completely remove f_1 from the equation. The system of equations is now closed. Now (4.18) is almost a regular diffusion equation except for the orbit-time-averaging performed on the RHS.

The lowest order distribution function, f_0 , only depends on u through \mathcal{E} , so the velocity derivative can be expressed as

$$\frac{\partial^2 f_0}{\partial u^2} = \left(\frac{\partial \mathcal{E}}{\partial u} \right)^2 \frac{\partial^2 f_0}{\partial \mathcal{E}^2} + \frac{\partial^2 \mathcal{E}}{\partial u^2} \frac{\partial f_0}{\partial \mathcal{E}} = u^2 \frac{\partial^2 f_0}{\partial \mathcal{E}^2} + \frac{\partial f_0}{\partial \mathcal{E}}. \quad (4.19)$$

Once again using the fact that f_0 only depends on t and \mathcal{E} , means that

$$\left\langle \frac{\partial^2 f_0}{\partial u^2} \right\rangle_{\mathcal{E}} = \langle v^2 \rangle_{\mathcal{E}} \frac{\partial^2 f_0}{\partial \mathcal{E}^2} + \frac{\partial f_0}{\partial \mathcal{E}}. \quad (4.20)$$

The next step is to use the thin boundary layer in a similar way as was done to derive (4.3). Using $\delta u \ll u$ with $\delta \mathcal{E} = u \delta u$ yields

$$\frac{\partial f_0}{\partial \mathcal{E}} \sim \frac{f_0}{u \delta u} \quad \text{and} \quad \frac{\partial^2 f_0}{\partial \mathcal{E}^2} \sim \frac{f_0}{(u \delta u)^2}, \quad (4.21)$$

so it is expected that

$$\langle v^2 \rangle_{\mathcal{E}} \frac{\partial^2 f_0}{\partial \mathcal{E}^2} \gg \frac{\partial f_0}{\partial \mathcal{E}}. \quad (4.22)$$

Using this assumption, (4.20) can be approximated by

$$\left\langle \frac{\partial^2 f_0}{\partial u^2} \right\rangle_{\mathcal{E}} \approx \langle v^2 \rangle_{\mathcal{E}} \frac{\partial^2 f_0}{\partial \mathcal{E}^2}. \quad (4.23)$$

This assertion must, however, be checked a posteriori once a solution has been found. This is done in section 4.3.3.

4.2.2 Calculating the orbit-time-averaged squared velocity

Since the constant energy contours are closed in region II and open in regions I and III, calculating an orbit-time-average differs slightly between the different regions.

Beginning with the open contour regions,

$$I_0 = \oint_{\mathcal{E}} d\vartheta = \oint \frac{dx}{v} = \frac{1}{\sqrt{2}} \oint \frac{dx}{\sqrt{\mathcal{E} - \psi(x)}}, \quad (4.24)$$

keeping in mind that \mathcal{E} is a constant in the integration.

To continue from here, $\psi(x)$ has to be known, by numerical computation, or approximated. From the forms found by the collisionless shock model, it is fair to say that in most cases $\psi(x)$ can be approximated as a sinusoidal plus a constant fairly well. Therefore, for the purpose of continuing the analytical treatment, assume

$$\psi(x) = \psi_{\min} + \psi_A \sin^2\left(\frac{\pi x'}{\lambda}\right). \quad (4.25)$$

The reason for using sine squared instead of just sine will become apparent soon. Also note that so far the convention has been that $\psi = \psi_{\max}$ at $x = 0$, but for convenience $x' = 0$ is here set at some point downstream where $\psi = \psi_{\min}$.

With this, (4.24) can be written as

$$\begin{aligned} I_0 &= \frac{1}{\sqrt{2}} \int_{-\lambda/2}^{\lambda/2} \frac{dx'}{\sqrt{\mathcal{E} - \psi_{\min} - \psi_A \sin^2(\pi x'/\lambda)}} \\ &= \frac{2\lambda}{\sqrt{2}\psi_A\pi k} \int_0^{\pi/2} \frac{d\theta}{\sqrt{1 - k^{-2} \sin^2 \theta}}, \end{aligned} \quad (4.26)$$

where the integration domain has been halved for an extra factor 2 since integrand is even in θ , and where

$$k := \sqrt{\frac{\mathcal{E} - \psi_{\min}}{\psi_A}}. \quad (4.27)$$

Note that $k \geq 1$ in regions I and III, while $k < 1$ in region II. This last integral can be expressed using the *complete elliptic integrals* [23, Sec. 19.2]

$$K(s) := \int_0^{\pi/2} \frac{d\theta}{\sqrt{1 - s \sin^2 \theta}}, \quad (4.28a)$$

$$E(s) := \int_0^{\pi/2} \sqrt{1 - s \sin^2 \theta} d\theta. \quad (4.28b)$$

The reader should note that some authors define the elliptic integrals with s^2 , rather than just s , on the RHS. Now, I_0 can be written as

$$I_0 = \frac{\sqrt{2}\lambda}{\pi\sqrt{\psi_A k}} K(k^{-2}). \quad (4.29)$$

Then the procedure is very similar for the other integral required,

$$\begin{aligned} \oint_{\mathcal{E}} 2(\mathcal{E} - \psi) d\vartheta &= \sqrt{2} \int_{-\lambda/2}^{\lambda/2} \sqrt{\mathcal{E} - \psi_{\min} - \psi_A \sin^2(\pi x'/\lambda)} dx' \\ &= \frac{2\sqrt{2}\psi_A k \lambda}{\pi} E(k^{-2}). \end{aligned} \quad (4.30)$$

Together this results in

$$2 \langle \mathcal{E} - \psi \rangle_{\mathcal{E}} \Big|_{k \geq 1} = 2\psi_A k^2 \frac{E(k^{-2})}{K(k^{-2})}, \quad (4.31)$$

in regions I and III where the constant energy contours are open.

In region II, where the orbits are closed, the procedure is a little bit more involved. The limits in x will have to be modified to $\pm\lambda_{\mathcal{E}}/2$, where $\lambda_{\mathcal{E}}$ is the width of the constant energy orbit in x at energy \mathcal{E} . This means that

$$\begin{aligned} J_0 &= \oint_{\mathcal{E}} d\theta = \frac{2}{\sqrt{2}} \int_{-\lambda_{\mathcal{E}}/2}^{+\lambda_{\mathcal{E}}/2} \frac{dx'}{\sqrt{\mathcal{E} - \psi_{\min} - \psi_A \sin^2(\pi x'/\lambda)}} \\ &= \frac{2\sqrt{2}\lambda}{\sqrt{\psi_A}\pi} \int_0^{+\theta_{\mathcal{E}}/2} \frac{d\theta}{\sqrt{k^2 - \sin^2 \theta}}. \end{aligned} \quad (4.32)$$

The extra factor 2 in front of the x' integral comes from the fact that the closed orbit has one curve with $u > 0$ and one curve with $u < 0$ for each x .

The trick for evaluating this last integral is to introduce the new variable φ such that $k \sin \varphi = \sin \theta$. Note that the integration limit $\lambda_{\mathcal{E}}/2$ corresponds to the point where $\psi(x') = \mathcal{E}$, or equivalently where $\sin \theta = k$; therefore $\theta = \theta_{\mathcal{E}}/2$ means that $\varphi = \pi/2$. Now the integration measure

$$d\theta = \frac{d\theta}{d\varphi} d\varphi = \frac{k \cos \varphi}{\sqrt{1 - k^2 \sin^2 \varphi}} d\varphi, \quad (4.33)$$

and the integrand

$$\sqrt{k^2 - \sin^2 \theta} = k \sqrt{1 - \sin^2 \varphi} = k \cos \varphi. \quad (4.34)$$

Together this results in

$$J_0 = \frac{2\sqrt{2}\lambda}{\sqrt{\psi_A}\pi} \int_0^{\pi/2} \frac{d\varphi}{\sqrt{1 - k^2 \sin^2 \varphi}} = \frac{2\sqrt{2}\lambda}{\sqrt{\psi_A}\pi} K(k^2). \quad (4.35)$$

Again the method is analogous, using (4.33) and (4.34), for the other integral

$$\begin{aligned}
 J_1 &= \oint_{\mathcal{E}} 2(\mathcal{E} - \psi) \, d\vartheta = \frac{4\sqrt{2\psi_A\lambda}}{\pi} \int_0^{\theta_{\mathcal{E}}/2} \sqrt{k^2 - \sin^2 \theta} \, d\theta \\
 &= \frac{4\sqrt{2\psi_A\lambda}}{\pi} \int_0^{\pi/2} \frac{k^2 \cos^2 \varphi}{\sqrt{1 - k^2 \sin^2 \varphi}} \, d\varphi.
 \end{aligned} \tag{4.36}$$

This can be solved by rewriting the numerator of the integrand as

$$k^2 \cos^2 \varphi = k^2 - k^2 \sin^2 \varphi = (k^2 - 1) + (1 - k^2 \sin^2 \varphi), \tag{4.37}$$

which translates into

$$J_1 = \frac{4\sqrt{2\psi_A\lambda}}{\pi} \left[(k^2 - 1)K(k^2) + E(k^2) \right]. \tag{4.38}$$

This now results in

$$2 \langle \mathcal{E} - \psi \rangle_{\mathcal{E}} \Big|_{k < 1} = \frac{J_1}{J_0} = 2\psi_A \left[\frac{E(k^2)}{K(k^2)} - 1 + k^2 \right]. \tag{4.39}$$

4.2.3 Arriving at a regular diffusion equation

Now, with $\langle \mathcal{E} - \psi \rangle_{\mathcal{E}}$ calculated, (4.18) can be expressed as

$$\frac{\partial \mathcal{f}_0}{\partial t} = 2\nu_* \psi_A k^2 F(k) \frac{\partial^2 \mathcal{f}_0}{\partial \mathcal{E}^2}, \tag{4.40}$$

where

$$F(k) = \begin{cases} k^{-2} \left[\frac{E(k^2)}{K(k^2)} + k^2 - 1 \right], & \text{for } k < 1, \\ \frac{E(k^{-2})}{K(k^{-2})}, & \text{for } k \geq 1. \end{cases} \tag{4.41}$$

To unify the variables on the RHS, the \mathcal{E} derivative is transformed into a k derivative, once again using the thin boundary layer argument,

$$\frac{\partial^2 \mathcal{f}_0}{\partial \mathcal{E}^2} = \left(\frac{\partial k}{\partial \mathcal{E}} \right)^2 \frac{\partial^2 \mathcal{f}_0}{\partial k^2} + \frac{\partial^2 k}{\partial \mathcal{E}^2} \frac{\partial \mathcal{f}_0}{\partial k} \approx \left(\frac{\partial k}{\partial \mathcal{E}} \right)^2 \frac{\partial^2 \mathcal{f}_0}{\partial k^2} = \frac{1}{4\psi_A^2 k^2} \frac{\partial^2 \mathcal{f}_0}{\partial k^2}. \tag{4.42}$$

With this, (4.40) becomes

$$\frac{\partial \mathcal{f}_0}{\partial t} = \frac{\nu_*}{2\psi_A} F(k) \frac{\partial^2 \mathcal{f}_0}{\partial k^2}, \tag{4.43}$$

which now only has k as the variable on the RHS.

The thin boundary layer is situated around $k = 1$. It is therefore natural to do a penultimate change of variables to $\varepsilon = 1 - k$, where $|\varepsilon| \ll 1$ in the region of interest, giving

$$\frac{\partial \mathcal{f}_0}{\partial t} = \frac{F(\varepsilon)}{\Upsilon^2} \frac{\partial^2 \mathcal{f}_0}{\partial \varepsilon^2}, \tag{4.44}$$

where

$$\Upsilon := \sqrt{\frac{2\psi_A}{\nu_*}} \gg 1. \quad (4.45)$$

The boundary layer is now around $\varepsilon = 0$. Now, introducing the final new variable w , defined such that

$$\frac{dw}{d\varepsilon} = \frac{\Upsilon}{\sqrt{F(\varepsilon)}}, \quad w(\varepsilon = 0) = 0, \quad (4.46)$$

turns (4.44) into

$$\frac{\partial \ell_0}{\partial t} = \frac{\partial^2 \ell_0}{\partial w^2}. \quad (4.47)$$

Once again the thin boundary layer argument has been used to neglect lower order derivatives of ℓ_0 .

The original perturbation equation, (4.9), has now finally be turned into a regular diffusion equation which can be solved analytically. The Green's function method gives the solution

$$\ell_0(t, w) = \int_{-\infty}^{\infty} dw' G(t, w - w') \ell_0(t = 0, w'), \quad (4.48)$$

with the Green's function for the diffusion equation is

$$G(t, \Delta w) = \frac{1}{\sqrt{4\pi t}} \exp\left(-\frac{(\Delta w)^2}{4t}\right). \quad (4.49)$$

In the collisionless limit, the distribution function drops discontinuously to zero on the separatrix, the initial condition can therefore be expressed as $\ell_0(t = 0, w) = \ell_i(v)\Theta(-w)$, where Θ is the Heaviside step-function, and with ℓ_i taken from (2.68). However since the boundary layer is so thin, variations due to $\ell_i(v)$ can be neglected to give

$$\ell_0(t = 0, w) = \mathcal{F}\Theta(-w), \quad (4.50)$$

with $\mathcal{F} = \ell_i(v \rightarrow -v_0)$. The solution, (4.48), can now be written down as

$$\begin{aligned} \ell_0(t, w) &= \frac{\mathcal{F}}{\sqrt{4\pi t}} \int_{-\infty}^{\infty} dw' \Theta(-w') \exp\left(-\frac{(w - w')^2}{4t}\right) \\ &= \frac{\mathcal{F}}{2} \operatorname{erfc}\left(\frac{w}{2\sqrt{t}}\right). \end{aligned} \quad (4.51)$$

Adding boundary conditions

While (4.51) is the formal solution to the diffusion equation with a step-function as the initial condition, it cannot be used directly here. For instance it will affect the distribution function even for $w < 0$ in region I, but region I is constantly refilled with more ions coming in from upstream. So instead ℓ_0^I , the distribution function in region I, is taken to be constant in time and is given by (2.68).

Next are regions II and III. There will still be an influx of ions from region I to II, and a subsequent outflux of ions from region II to III. So since (4.51) with any constant factor still solves the diffusion PDE (4.47), it can be used instead with the boundary conditions $\ell_0^{\text{II}}(\mathcal{E}, w = 0) = \mathcal{F}$ and $\ell_0^{\text{II}}(\mathcal{E}, w \rightarrow \infty) = 0$. The second boundary condition not quite rightly posed, since w never reaches ∞ in region II. However, it can be thought of as a boundary condition if region II were to be extended to $w \rightarrow \infty$. Now, since ℓ_0^{II} solves (4.47) and satisfies the boundary conditions, it must also be the unique solution to this linear problem. That was however only the $v < 0$ part of region II; and since the orbit time scales are much shorter than the collisional time scales, the $v > 0$ part of region II is set to be mirrored¹ that of the $v < 0$ part.

Then lastly considering region III. Since the distribution function in region II has the value \mathcal{F} on the boundary, the same boundary condition for $w = 0$ should be imposed on ℓ_0^{III} . Therefore choose ℓ_0^{III} the same as ℓ_0^{II} , but with opposite sign in the erfc function, since w is decreasing when moving away from the separatrix into region III. Obviously the different sign in the erfc does not affect the fact that ℓ_0^{III} is still a solution to the diffusion PDE, since (4.47) only has a second derivative in w .

To summarize,

$$f^{\text{II}}(t, w) = \mathcal{F} \operatorname{erfc}\left(\frac{w}{2\sqrt{t}}\right), \quad (4.52a)$$

$$\text{and } f^{\text{III}}(t, w) = \mathcal{F} \operatorname{erfc}\left(\frac{-w}{2\sqrt{t}}\right), \quad (4.52b)$$

where

$$\mathcal{F} = \ell_i(v \rightarrow -v_0) = n_{i,0} \sqrt{\frac{\tau_i}{2\pi}} \exp\left[-\frac{\tau_i}{2} \left(\sqrt{2\psi_{\max}} - \mathcal{M}\right)^2\right] \quad (4.53)$$

in order to make the distribution function continuous over the boundaries.

4.2.4 The density of diffused ions

To study how the collisions affect the shock, the ion density has to be calculated. Now that the diffused distribution function is known, the density of the diffused ions can easily be calculated. These calculations are done separately for regions II and III.

Region III

Beginning with the particle density in region III,

$$n^{\text{III}} = \int_{v_0}^{\infty} dv \ell^{\text{III}}(v) = \mathcal{F} \int_{v_0}^{\infty} dv \operatorname{erfc}\left(-\frac{w(v)}{2\sqrt{t}}\right). \quad (4.54)$$

¹While not immediately obvious, v and $-v$ are actually represented by the same w coordinate. This is because w is ultimately derived from \mathcal{E} , and \mathcal{E} is even in v .

Then going to energy $\mathcal{E} = \frac{1}{2}v^2 + \psi$ as the integration variable,

$$n^{\text{III}} = \frac{\mathcal{F}}{\sqrt{2}} \int_{\psi_{\text{max}}}^{\infty} \text{erfc}\left(-\frac{w(\mathcal{E})}{2\sqrt{\mathcal{E}}}\right) \frac{d\mathcal{E}}{\sqrt{\mathcal{E} - \psi_{\text{min}} + q_{\psi}^2 \psi_A}}, \quad (4.55)$$

where

$$\psi_A = \psi_{\text{max}} - \psi_{\text{min}} \quad \text{and} \quad q_{\psi} = \sqrt{\frac{\psi - \psi_{\text{min}}}{\psi_A}}. \quad (4.56)$$

This yields

$$n^{\text{III}} = \mathcal{F} \sqrt{2\psi_A} \int_1^{\infty} \text{erfc}\left(-\frac{w(k)}{2\sqrt{\mathcal{E}}}\right) \frac{k dk}{\sqrt{k^2 - q_{\psi}^2}}. \quad (4.57)$$

Note that while $k = 1$ on the separatrix, $q_{\psi}^2 \geq 1$ with equality only at the crossings of the separatrices, i.e. where $\psi = \psi_{\text{max}}$.

Region II

The procedure for region II is quite similar, but with some key differences. Firstly the integration limits will have to be $\pm v_0$,

$$n^{\text{II}} = \int_{-v_0}^{v_0} dv \mathcal{F}^{\text{II}}(v) = 2 \int_0^{v_0} dv \mathcal{F}^{\text{II}}(v). \quad (4.58)$$

Then going to \mathcal{E} as the integration variable is just as before in (4.55), but now with the integration limits $\mathcal{E} = \psi$ to $\mathcal{E} = \psi_{\text{max}}$, which then yields the k integral

$$n^{\text{II}} = 2\mathcal{F} \sqrt{2\psi_A} \int_{q_{\psi}}^1 \text{erfc}\left(\frac{w}{2\sqrt{\mathcal{E}}}\right) \frac{k dk}{\sqrt{k^2 - q_{\psi}^2}}. \quad (4.59)$$

Quasi-neutrality and the electron density

Since the collisions affect the ion density, the electron density has to be modified as well, to keep quasi-neutrality at the far upstream end. This is easily done by simply adding the contribution from region III with $\psi = 0$,

$$n_{i,2} = \mathcal{F} \sqrt{2\psi_A} \int_1^{\infty} \text{erfc}\left(-\frac{w}{2\sqrt{\mathcal{E}}}\right) \frac{k dk}{\sqrt{k^2 + \psi_{\text{max}}/\psi_A}}, \quad (4.60)$$

to the far upstream electron density (2.75).

4.3 Studying the new variable

So far the result in (4.52) is expressed in the, somewhat obscure, variable w while the physics lies in the velocity, v , or the energy, \mathcal{E} . Therefore, this section will deal with how to find the form of $w(\varepsilon)$, from which the energy or velocity dependence can be recovered. Asymptotic expansions for w will be presented in the following subsection, these can then be used to find a suitable approximation function for $w(\varepsilon)$, and then to also verify dropping the first order derivatives in the derivation of the model, which are done in the subsequent subsections.

As an initial comment, it is clear from the definition of w , (4.46), that $\Upsilon \propto \nu_*^{-1/2}$ only acts as a scale factor for w . Then, since w is only used in conjunction with $\mathcal{E}^{-1/2}$, as in (4.52), ν_* and \mathcal{E} will also only appear together as the product $\mathcal{E}\nu_*$. The individual values of \mathcal{E} and ν_* are therefore not of any significant interest in this model. Of course in reality, that is not the case since other effects can affect the shock and its time evolution.

4.3.1 Asymptotic expansions for $w(\varepsilon)$

In this subsection an asymptotic formula for $w(\varepsilon)$ as $\varepsilon \rightarrow 0$, is presented. The reader should therefore be aware of the more strict use of the symbol “ \simeq ”. In this thesis \simeq means that the RHS approaches the LHS faster than the smallest term on either side. That is, in this context \simeq signifies a *proper asymptotic approximation*, and should not be confused with \sim which is just an order of magnitude estimate. For some more detail on asymptotic methods, the reader is referred to the book by Lin and Segel [24].

Small ε limit

With $w(\varepsilon)$ defined by (4.46), it can be expressed as

$$w(\varepsilon) = \Upsilon \int_0^\varepsilon \frac{d\varepsilon'}{\sqrt{F(\varepsilon')}}. \quad (4.61)$$

Using the asymptotic expansions for the complete elliptic integrals [23, Sec. 19.12]

$$K(k^{\pm 2}) \simeq \frac{1}{2} \ln\left(\frac{1}{|\varepsilon|}\right) + \frac{3}{2} \ln(2) + \mathcal{O}(\varepsilon) \quad (4.62a)$$

$$E(k^{\pm 2}) \simeq 1 + \mathcal{O}(\varepsilon), \quad (4.62b)$$

for $k = 1 - \varepsilon$ as $\varepsilon \rightarrow 0$, the asymptotic expansion for $F(\varepsilon)$ becomes

$$F(\varepsilon) \simeq \frac{2}{\ln(8/|\varepsilon|)} \quad \text{as } \varepsilon \rightarrow 0. \quad (4.63)$$

The $\mathcal{O}(\varepsilon)$ is omitted from now on for brevity. Using this expansion in (4.61) yields

$$\frac{w(\varepsilon)}{\Upsilon} \simeq \frac{\varepsilon}{\sqrt{2}} \sqrt{\ln\left(\frac{8}{|\varepsilon|}\right)} \pm 2\sqrt{2\pi} \operatorname{erfc}\left(\sqrt{\ln\left(\frac{8}{|\varepsilon|}\right)}\right) \quad \text{as } \varepsilon \rightarrow 0^\pm. \quad (4.64)$$

Note that, for $|\varepsilon| \lll 1$, the erfc term is around two orders of magnitude smaller than the first term, but the erfc term provides a valuable extension of the range for which this expansion is valid. Also note that while (4.63) seems sign independent, the absolute value should be read as $|\varepsilon| = \pm\varepsilon$ which is the reason for the \pm in (4.64). This therefore means that both terms always have the same sign.

Large $|\varepsilon|$ limit

Then there are the limits away from $\varepsilon = 0$. At first this seems like a strange limit to be interested in, since ε has so far been said to always be very close to zero. However later, when determining the density of diffused ions, the resulting integrals are taken over large intervals in ν , and hence also large intervals in ε . In these limits, the asymptotic behavior differ between positive and negative ε , so they will be treated separately.

First the limit $\varepsilon \rightarrow 1$, or equivalently $k \rightarrow 0$. Using the expansions of the elliptic integrals for small k given in [23, Sec. 19.5], (4.46) becomes

$$\frac{1}{\Upsilon} \frac{dw}{d\varepsilon} \simeq \frac{1}{\sqrt{\frac{1}{2} - \frac{k^2}{16}}} \simeq \sqrt{2} \left(1 + \frac{k^2}{16} \right) \quad \text{as } k \rightarrow 0. \quad (4.65)$$

Which, using $k = 1 - \varepsilon$, results in

$$\frac{w(\varepsilon)}{\Upsilon} \simeq \sqrt{2}(\varepsilon - 1) - \frac{\sqrt{2}}{48}(1 - \varepsilon)^3 + C^+, \quad (4.66)$$

where C^+ is some unknown constant of integration which can be determined, by numerically calculating $w(\varepsilon = 1)$ and then matching that value against the asymptotic value above.

Then the limit $\varepsilon \rightarrow -\infty$, which, again using [23, Sec. 19.5], yields²

$$\frac{w(\varepsilon)}{\Upsilon} \simeq 1 \quad \text{as } \varepsilon \rightarrow -\infty. \quad (4.67)$$

This then gives

$$\frac{w(\varepsilon)}{\Upsilon} \simeq \varepsilon + C^-, \quad (4.68)$$

for some other integration constant C^- . This time however, C^- cannot be calculated as naturally as before since w is not finite in the limit $\varepsilon \rightarrow -\infty$; instead $w(\varepsilon)$ has to be calculated for a sufficiently large (negative) ε , from which the above asymptotic expansion is matched.

²When implementing the result of this calculation in the approximation function \hat{w} , described below, it was found that a higher order approximation could not be used at $\varepsilon = -2$, which is the upper limit for which this asymptotic expansion is used.

4.3. Studying the new variable

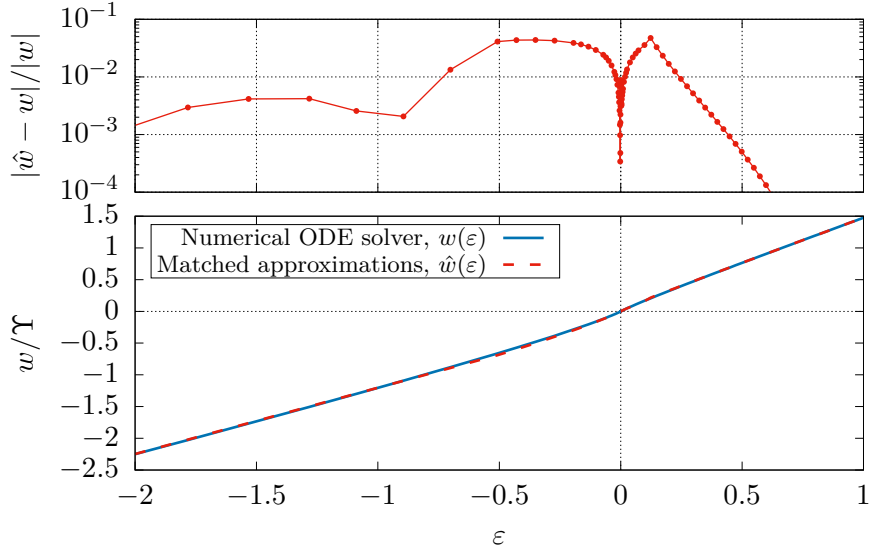


Figure 4.2: The variable w as a function of the kinetic variable ε . Note that the variable on the vertical axis is w/Υ , where $\Upsilon = \sqrt{2\phi_A/\nu_*} \gg 1$. Also shown here is the relative error of the approximation of w , \hat{w} , used in the following numerical calculations.

4.3.2 Returning to the original variables – numerical approach

The results in (4.64), (4.68), and (4.66) are only asymptotically valid in either limit of ε . Unfortunately the only analytical refinement possible is to include more terms in the asymptotic expansions, and even that might not help since not all asymptotic series are convergent. Instead numerical methods have to be employed. One way to numerically compute $w(\varepsilon)$ is to simply use the definition of w , (4.46),

$$\frac{1}{\Upsilon} \frac{dw}{d\varepsilon} = \frac{1}{\sqrt{F(\varepsilon)}}, \quad w(\varepsilon = 0) = 0. \quad (4.69)$$

This is a first order ODE, which can easily be solved numerically, with for instance a Runge-Kutta method. It is also noted that the only role Υ plays here is that of a scale factor for w ; numerical calculations of $w(\varepsilon)$ can therefore be performed with $\Upsilon = 1$, and then scaled by the desired value of Υ .

There are however some details which need a bit of extra attention. The first and foremost being that the initial condition $w(0) = 0$ cannot be used in the numerical solver, since $F(0) = 0$ the derivative is ill-behaved at $\varepsilon = 0$. This is where the work with the asymptotic expansion comes into play. Instead of starting at $(\varepsilon, w) = (0, 0)$, the numerical solver can be given a starting point (ε_0, w_0) , with $\varepsilon_0 \ll 1$ and then w_0 is given by (4.64). Using this method, with $\varepsilon_0 = 1 \times 10^{-15}$, $w(\varepsilon)$ has been plotted in Figure 4.2.

In order to effectively use $w(\varepsilon)$ in later numerical methods, an approximation function, $\hat{w}(\varepsilon)$ has been utilized. For positive ε , $\hat{w}(\varepsilon)$ is first given by (4.64) for $0 < \varepsilon \leq 0.1$ and then

given by (4.66) with $C^+ = 1.4756$ for $0.1 < \varepsilon \leq 1$. Then for negative ε , the approximation function is divided into three parts with breaking points at $\varepsilon = -0.5$ and -2 . In the first part, $-0.5 \leq \varepsilon < 0$, (4.64) is used, then the lowest region, $\varepsilon \leq -2$, (4.68) is used with $C^- = -0.3310$ based on a numerical calculation of $w(\varepsilon = -50)/\Upsilon = -50.3310$. Then for $-2 < \varepsilon < -0.5$, a linear curve connecting the two asymptote is used. The result of this approximation function, \hat{w} , is shown as the dashed curve in the lower panel of Figure 4.2, as well as a graph of the relative error $|(\hat{w} - w)/w|$ in the upper panel. The relative error stays below 5%.

4.3.3 A posteriori verification of previous assumptions

In the calculations leading up to the results above, the thin boundary layer argument has been used freely to neglect lower order derivatives in ν , \mathcal{E} , and k along the way. These assumptions will be checked here.

It is now clear that the width of the boundary layer in w is $\delta w \sim \sqrt{\ell}$. This means that the boundary layer width in terms of ε is $\delta\varepsilon \sim \sqrt{\ell}/\Upsilon \sim \sqrt{\ell\nu_*}$, which can be seen from the relation between w/Υ and ε in Figure 4.2. Of course the width in k is the same as in ε , $\delta k = \delta\varepsilon$. Then using the definition of k , (4.27),

$$\delta\mathcal{E} = 2\psi_A k \delta k \sim k \sqrt{2\ell\psi_A\nu_*} \sim \sqrt{\ell\nu_*} \ll 1, \quad (4.70)$$

recalling that $k = 1$ at the boundary. These are the estimates of the boundary layer widths which can now be used to check the relative sizes of the first and second derivatives.

Beginning with the first change of variables subject to an approximation of this kind, (4.20), which can be exactly written as

$$\left\langle \frac{\partial^2 \mathcal{f}_0}{\partial \nu^2} \right\rangle_{\mathcal{E}} = 2\psi_A k^2 F(k) \frac{\partial^2 \mathcal{f}_0}{\partial \mathcal{E}^2} + \frac{\partial \mathcal{f}_0}{\partial \mathcal{E}}. \quad (4.71)$$

While in most cases $\nu \sim 1$, on the separatrix, where $\nu = \pm\nu_0$, that is not necessarily the case, especially on points where $\psi \rightarrow \psi_{\max}$ and $\nu_0 \rightarrow 0$. This also results in $\langle \nu^2 \rangle \rightarrow 0$ on the whole of the separatrix, which violates the assumption that the first derivative could be neglected compared to the second derivative. However, as shall soon be apparent, this violation only becomes important in an *extremely* narrow region near the separatrix. This region is narrow even compared to the rates of change of \mathcal{f}_0 , meaning that even though the assumptions are violated the contribution from this region is still so small that the overall behavior of \mathcal{f}_0 is not affected. This line of reasoning is very similar to the one used by Hazeltine et al. in [25].

To show that the region of violation is as narrow as claimed, let $\hat{\delta\varepsilon}$ denote the width of this region. In this region the two terms in (4.71) are of comparable size, meaning that

$$F(\hat{\delta\varepsilon}) \frac{\mathcal{f}_0}{(\delta\mathcal{E})^2} \sim \frac{\mathcal{f}_0}{\delta\mathcal{E}}. \quad (4.72)$$

Using the asymptotic expansion of $F(\varepsilon)$, (4.63), yields

$$\frac{1}{-\ln(|\hat{\delta\varepsilon}|)} \sim \delta\mathcal{E} \sim \sqrt{\ell\nu_*}, \quad (4.73)$$

or equivalently

$$|\hat{\delta}\varepsilon| \sim \exp\left(-\frac{1}{\sqrt{t\nu_*}}\right) \lll \delta\varepsilon, \quad (4.74)$$

which is exponentially small, since $t\nu_* \ll 1$. Any contribution to ℓ_0 from this region, $\hat{\delta}\ell_0$, will only be approximately $\hat{\delta}\varepsilon/\delta\varepsilon \lll 1$. Thus, neglecting the first order \mathcal{E} -derivative will not affect the end result, even though the approximation formally breaks down very near the separatrix. The other first order derivatives that have been neglected in the derivation of the collisional distribution function can also be treated in a similar way.

4.4 Numerical implementation

Just as with the previous shock models this model will need to be studied numerically as well. In this section the numerical implementation is briefly described.

The numerical implementation of this model is very similar to what has been described in section 3.1, but with the diffused ion densities from above added in the code. The integrations in (4.57), (4.59), and (4.60) were performed using the approximation function described in section 4.3.2.

To help the numerical integration, an upper integration limit

$$k_{\max} = 1 + \frac{10\sqrt{t}}{\Upsilon}. \quad (4.75)$$

is imposed on (4.57) and (4.60) in the numerical implementation. The choice of this limit is based on the fact that the width, in terms of w , of the boundary layer in which ℓ_0 has an appreciable value is $\delta w \sim \sqrt{t}$, which since $\delta\varepsilon \sim \Upsilon\delta w$ corresponds to a width in k of $\delta k = \delta\varepsilon \sim \sqrt{t}/\Upsilon$; then an extra factor of 10 is used as a margin. Any contribution to n^{III} outside this k_{\max} is extremely small due to the nature of the erfc function.

In this model, like the AD electron trapping model, ψ_{\min} as well as ψ_{\max} have to be calculated together in a system of equations like (3.1). Furthermore, there are more numerical integrations in this model, and the new integrands are not always that well behaved, since they sometimes have singularities at the integration limits. Due to these issues the runtime is negatively affected. The runtime of finding a single shock can now reach several minutes. This do however almost exclusively happen for large $t\nu_* \sim 0.1$, after which the model usually breaks down anyway; at $t\nu_* \sim 10^{-3}-10^{-2}$ the runtimes are still at around 10s per shock object. Again these runtimes are on a single core in a medium to high end workstation PC.

As with the collisionless code, the Matlab packages used in the implementation of this model are available on GitHub³.

4.5 The effects of collisions

When studying the collisions here, only Maxwell-Boltzmann electrons have been considered. The results of these studies are presented in this section.

³https://github.com/andsunds/Shock_pkg

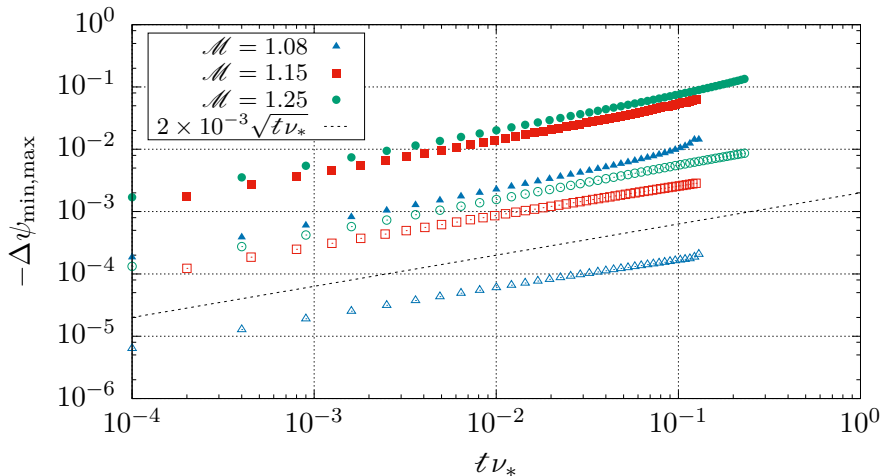


Figure 4.3: Log-log plot of the of $-\Delta\psi_{\min}$ (solid markers) and $-\Delta\psi_{\max}$ (open markers) from a collisional shock as a function of time. All shocks are calculated with $\tau_i = 50$. The slopes are all in the ranges 0.5–0.6 (the dotted line has a slope of 0.5 for comparison), indicating a slightly faster than square root of t dependence. Note that the few highest data points for $\mathcal{M} = 1.08$ are unphysical since ψ_{\min} has reached 0 and the model has broken down there.

The time dependence of the solutions have been studied for single ion species shocks at three different Mach numbers at $\tau_i = 50$. Both ψ_{\max} and ψ_{\min} are found to decrease with time, so Figure 4.3 shows the change in ψ_{\min} and ψ_{\max} ,

$$-\Delta\psi_{\min,\max} = \psi_{\min,\max}(0) - \psi_{\min,\max}(t). \quad (4.76)$$

Note the log-log scale in Figure 4.3 and how the data points fall on almost straight lines. All the sets of data points have a slope of 0.5–0.6, indicating that $\Delta\psi_{\min,\max} \propto -\sqrt{t\nu_*}$, which is very interesting but somewhat expected. It was expected since the basis for this model is a type of diffusion equation, and the solutions of diffusion equations usually exhibit \sqrt{t} behaviors in some form or another. In fact, a surprisingly similar method has been used by Fülöp et al. [26] to study collisional effects on fusion plasmas, and they similarly found a $\sqrt{\nu_*}$ dependence. The result here is however still interesting since the patterns are so consistent – the only expected part was that if a pattern would appear at all, then it would be \sqrt{t} .

It is also interesting to note that the values of $-\Delta\psi_{\max}$ are around an order of magnitude smaller than those of the corresponding $-\Delta\psi_{\min}$. This means that while the collisions do affect the downstream of the shock, ψ_{\max} is not affected very much. As a consequence of that the upstream region of the shock is not affected significantly by the collisions, neither is the ion reflection since that is governed by $F_i := 2\psi_{\max}/\mathcal{M}^2$ according to Appendix A.

The effect of collisions on the form of the shock and the charge density is shown in Figure 4.4, which show the initial shock, at $t\nu_* = 0$, and later when the collisions have

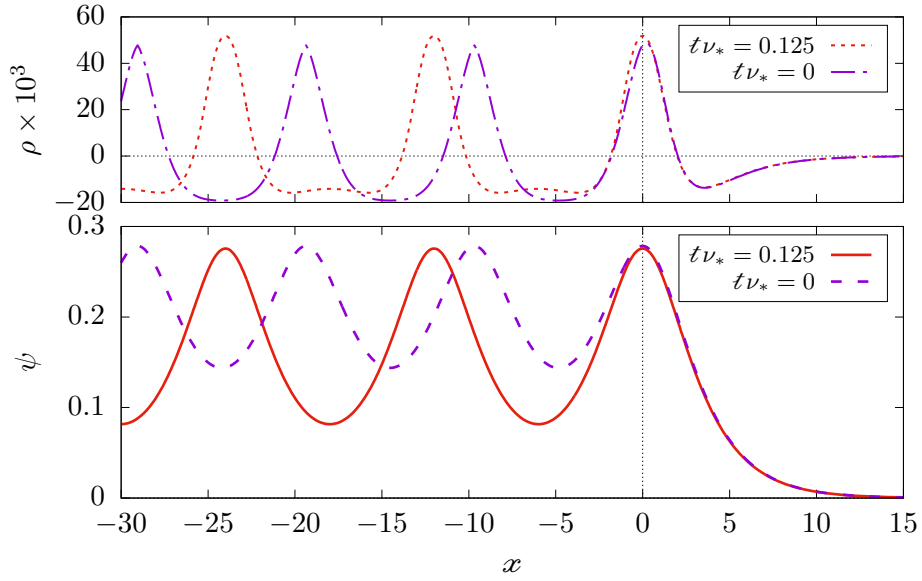


Figure 4.4: Comparison between a collisionless ($t\nu_* = 0$) and a collisional shock after a time $t\nu_* = 0.125$ has passed. These two shocks correspond to the first and last shock of the series of shocks in Figure 4.3. The lower panel shows the electrostatic potential of each shock, while the upper panel shows their charge density.

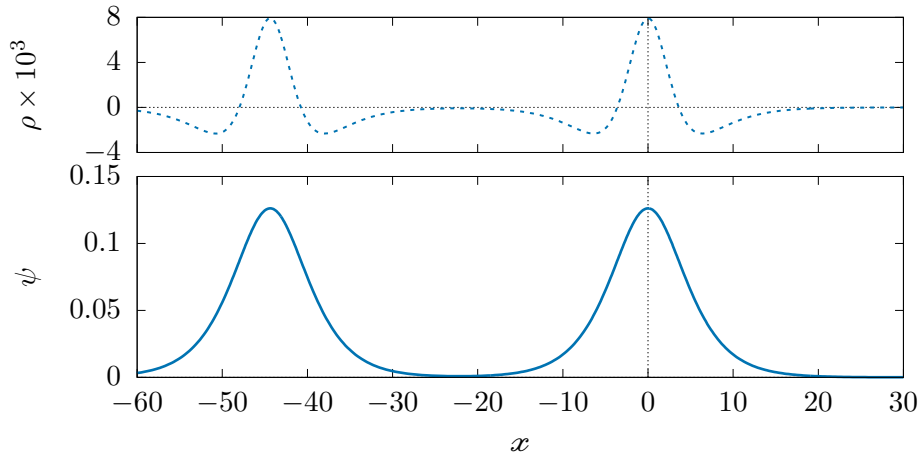


Figure 4.5: The extreme limit of the collision model, showing the charge density, ρ , and potential, $\psi(x)$, for a shock with $\tau_i = 50$, $\mathcal{M} = 1.08$, and $t\nu_* = 0.120$. This is right before the model breaks down completely.

had time to significantly modify the charge density, at $t\nu_* = 0.125$. The fact that ψ_{\min} is affected much more than ψ_{\max} is clear from this figure. Figure 4.4, showing $\rho(x)$, also reveals that the downstream oscillations are not very sinusoidal, otherwise $\rho = -d^2\psi/dx^2$ would have also been sinusoidal; the deviation from a sinusoidal spatial dependence is also growing with time. This means that the assumption made in (4.25) does not quite reflect reality in cases like this where the amplitude of the downstream oscillation is rather large. The deviation from sinusoidal oscillations is however only clearly visible in the second derivative, and not in $\psi(x)$ itself. This will therefore most likely not affect the results very much for these shocks.

Of course the square root of time dependence cannot continue indefinitely. This is illustrated in the time series for $\mathcal{M} = 1.08$ in Figure 4.3, where the last few data points show that $-\Delta\psi_{\min}$ first starts increasing faster and then abruptly flattens out. This sudden stop in the change of $-\Delta\psi_{\min}$ is due to the fact that ψ_{\min} has reached 0 and can no longer continue decreasing. The form of the potential $\psi(x)$ and the charge density ρ of a shock just before this happens is shown in Figure 4.5. While the deviation from sinusoidal oscillation was not that great in Figure 4.4, in Figure 4.5 the deviation from a sinusoidal is definitely a problem here, and the theoretical model cannot be expected to hold this far. This illustrates an important limitation to this model, i.e. that it can only be said to be valid for small enough $t\nu_*$ and that in turn depends on the initial form of the shock; at low Mach numbers, where ψ_{\max} and ψ_{\min} are low initially, the model breaks down quicker than at high Mach numbers, where the initial ψ_{\max} and ψ_{\min} are larger.

There are however some important features that are still qualitatively valid, even for these degenerated oscillation shapes. The inverse logarithmic behavior of $F(\varepsilon)$ for $\varepsilon \ll 1$, (4.63), is still valid – albeit with some other constants. This is because $d^2\psi/dx^2 = -\rho(x)$ is still continuous and non-zero at the peaks, meaning that the orbit-time-averages in section 4.2.2 will still have their logarithmic divergence. This means that the qualitative behavior of w near the boundary will be more or less unaffected, leading to similar end results.

4.6 Possible extensions and improvements

The collisional shock model presented here in this thesis is an important first step, but it still has room for improvement. Some points on how to further develop this model are raised and discussed in the following.

The perhaps easiest extension of this model is to also include effects of electron trapping, together with collisions. No significant theoretical work is needed to do this, and it would most likely only involve fusing the different parts of code from the different models. Since both electron trapping and ion collisions act to increase the amplitude of the oscillations it would be interesting to see the effects together. An interesting point to study would be to see how collisions affect an AD shock in a region with multiple solutions, e.g. from Figure 3.4; one might perhaps find that some of the solutions are unstable.

One issue mentioned already in section 4.1.1, is the mathematically and physically somewhat unjustified assumption to neglect any velocity dependence of ν_* . This was

motivated to simplify the theory in this early stage. It is however not unfeasible to redo the derivation with a velocity dependent ν_* . To do this, firstly ν_* has to be specified by a more careful study of the collision operator, and secondly the integrals in section 4.2.2 must be redone with $\langle 2\nu_* v^2 \rangle$ instead. This would of course change the results somewhat, but the qualitative results presented above are not expected to change very much.

As of now this model does not take all the aspects of the scattered ions into account. By enforcing that \mathcal{I}^I is constant in time everywhere, this model does not take into account that the ions scattered into region II must also have left region I. It is true that region Ia is continuously refilled at the shock front, and \mathcal{I}^I should reasonably be considered constant in time, but further downstream \mathcal{I}^I has to decrease if the number of ions is to be conserved. This does however break one of the main assumptions of this model that \mathcal{I}_0 is periodic in the downstream. One possible way to handle this is to say that this variation in x happens on a much longer length scale, on the order of magnitude ν_*^{-1} , than the size of each particular island of trapping, so that the orbit-time-average for each particular island is similar to what is done here but differs between island, i.e. $\langle \cdot \rangle_{\mathcal{E}} \rightarrow \langle \cdot \rangle_{\mathcal{E}}^i$ where the index i denotes which island the orbit-time-average is taken at. A treatment like this would likely result in a spacial attenuation of the downstream oscillation amplitude, as there will be fewer ions trapped on each successive island. It should however be emphasized again that, except in extreme cases like in Figure 4.5, the collision model at its present stage still provides a good approximation near the shock front.

Another very interesting and relevant point regarding collisions is how multiple ion species or impurity ions affect the results of collision. Some of the major work required to generalize to multiple ion species lies in the need to now consider inter-species collisions and drag forces exerted between the different species. It is a non-trivial work to do this generalization. Inter-species collisional effects have, in simulations, been shown to be able to cause very fast heating of the light ions [9].

Chapter 5

Conclusions

In this thesis, a semi-analytical model of electrostatic shocks is presented and further developed. Effects of electron trapping are studied using two different models. Also the effects of a weak but finite ion collisionality are studied through a semi-analytical, time dependent model developed in this thesis.

The effects of electron trapping have been modeled as a flattening of the electron distribution function in the trapping regions of phase space. The two models of the electron trapping only differ in the sizes of the trapping regions. By flattening out the electron distribution function in the trapped regions, the electron density is in fact lowered compared to a Boltzmann response. This lowering of the electron density shifts the total charge density toward being more positive, which results in generally larger amplitudes of the downstream oscillation.

Depending on how the shock was created, the far downstream of shock might be very different. That is why two models for the effects of electron trapping were considered. The first model had a freely set potential threshold, above which the electrons were assumed to be trapped, and the other model had the threshold strictly set by the downstream potential oscillations. To further study this phenomenon, more knowledge on the far downstream conditions of the shock is required. In the second model, multiple shock solutions are found for the same input parameters in certain parameter regions. It would be very interesting to study the stability of the different solutions to determine which type of solution will be more likely to be found in an experiment.

To model collisions in the shock, an orbit-time-averaging technique has been employed to find the leading order perturbative solution to the kinetic equation, in the smallness of the collisionality. As the passing ions are continuously refilled by incoming ions, the passing ion distribution function is assumed to be unaffected by the collisions. Meanwhile more and more ions are scattered into other regions of phase space, smoothing out the previous discontinuity of the distribution function. Since ions get trapped, the charge density is again shifted towards being more positive; hence the effects of collisions are somewhat similar to those of electron trapping. However the collisional model has a time dependence which the electron trapping model lacks. Very interestingly, the amplitude of the downstream oscillations grow as the square root of time, but the maximum value of

the potential is more or less unaffected.

This collisional shock model is only a first step, and as such it has a few limitations and uses a model collision operator. One of the limitations that occur during time evolution of the model is that the model breaks down when enough ions have been scattered into the trapping regions of phase space. This is because the scattered ions not only affect the amplitude of the downstream oscillation, but also its shape; therefore some of the assumptions made to derive the model break. This happens without any prior warning. However, it is stressed that the model, as it is presented here, is still valid early on in the time evolution.

Besides adjusting the model to handle this limitation, there are several other possible ways to improve upon this model. For instance, another collision operator could be used, or a spatial downstream dependence could be studied. The perhaps easiest extension of the work in this thesis would be to combine the ion collisions with electron trapping; both models have similar effects on the downstream oscillations, and it would be interesting to study how they interact.

On a larger scale it would be desirable to extend the semi-analytical model to higher dimensions to be able to also include effects of magnetic fields. This is crucial for the development of a model of shocks which can be used for ion acceleration purposes. The electrostatic shocks only have a limited range of shock propagation speeds, as has been seen in chapter 3, and can therefore not be used to accelerate ions to very high energies. Meanwhile magnetized shocks does not have an upper speed limit [27] – except the speed of light. However the Sagdeev potential method does unfortunately only work with a one dimensional theory, so some other means of finding the form and shape of the shock front is required. Also, relativistic effects will have to be considered if high energy acceleration is to be considered.

Another pressing issue is that of time evolution. The collisional model does have a time dependency due to collisions, but other types of time dependencies definitely exist. For instance, shocks are dissipative, but at this stage the model does not take energy transfer from the field into the reflected ions into account, which in some circumstances might affect the shock. Closely related to the time evolution issue is the problem of shock formation. There is presently no good understanding of the formation stage of shocks, which would be of great importance for any intended application of shocks.

Bibliography

- [1] D. A. Tidman and N. A. Krall, *Shock waves in Collisionless Plasmas*, Wiley Series in Plasma Physics, Wiley-Interscience (1971), ISBN 0-471-86785-3.
- [2] A. Macci, *A Superintense Laser-Plasma Interaction Theory Primer*, Springer (2013), ISBN 978-94-007-6124-7.
- [3] A. Marcowith, A. Bret, A. Bykov, M. E. Dieckman, L. O. Drury, B. Lembège, M. Lemoine, G. Morlino, G. Murphy, G. Pelletier, I. Plotnikov, B. Reville, M. Riquelme, L. Sironi, and A. S. Novo, “The microphysics of collisionless shock waves,” *Reports on Progress in Physics* **79**, 046901 (2016).
- [4] D. Haberberger, S. Tochitsky, F. Fiuza, C. Gong, R. A. Fonseca, L. O. Silva, W. B. Mori, and C. Joshi, “Collisionless shocks in laser-produced plasma generate monoenergetic high-energy proton beams,” *Nature Physics* **8** pp. 95–99 (2012).
- [5] A. Balogh and R. A. Treumann, *Physics of Collisionless Shocks*, vol. 12 of *ISSI Scientific Report*, Springer (2013), ISBN 978-1-4614-6099-2.
- [6] F. S. Mozer, C. W. Carlson, M. K. Hudson, R. B. Torbert, B. Parady, and J. Yatteau, “Observations of paired electrostatic shocks in the polar magnetosphere,” *Physical Review Letters* **38** pp. 292–296 (1977).
- [7] J. Vink, “Supernova remnants: the X-ray perspective,” *The Astronomy and Astrophysics Review* **20** p. 49 (2011).
- [8] D. W. Swift, “Acceleration mechanisms for auroral electrons,” *Journal of Geomagnetism and Geoelectricity* **30** pp. 449–459 (1978).
- [9] A. E. Turrell, M. Sherlock, and S. J. Rose, “Ultrafast collisional ion heating by electrostatic shocks,” *Nature Communications* **6**, 8905 (2015).
- [10] R. A. Cairns, R. Bingham, P. Norreys, and R. Trines, “Laminar shocks in high power laser plasma interactions,” *Physics of Plasmas* **21**, 022112 (2014).
- [11] R. A. Cairns, R. Bingham, R. Trines, and P. Norreys, “Weak collisionless shocks in laser-plasmas,” *Plasma Physics and Controlled Fusion* **57**, 044008 (2015).

-
- [12] I. Pusztai, J. M. TenBarge, A. N. Csapó, J. Juno, A. Hakim, L. Yi, and T. Fülöp, “Low Mach-number collisionless shocks and associated ion acceleration,” *Plasma Physics and Controlled Fusion* **60**, 035004 (2018).
- [13] J. Billingham and A. C. King, *Wave Motion*, Cambridge texts in Applied Mathematics, Cambridge University Press (2000), ISBN 0-521-63257-9.
- [14] K. van der Weele and G. Kanellopoulos, “Coexistence of up- and downstream traffic waves on a ring road,” *European Physical Journal Special Topics* **225** pp. 1127–1141 (2016).
- [15] A. C. Scott, *The Nonlinear Universe*, The Frontiers Collection, Springer (2007), ISBN 978-3-540-34152-9.
- [16] F. F. Chen, *Introduction to Plasma Physics and Controlled Fusion*, Springer, 3 ed. (2016), ISBN 978-3-319-22308-7.
- [17] A. Piel, *Plasma Physics, An Introduction to Laboratory, Space, and Fusion Plasmas*, Springer (2010), ISBN 978-3-642-10491-6.
- [18] S. S. Moiseev and R. Z. Sagdeev, “Collisionless shock waves in a plasma in a weak magnetic field,” *Journal of Nuclear Energy C* **5** pp. 43–47 (1963).
- [19] R. Z. Sagdeev, “Cooperative phenomena and shock waves in collisionless plasmas,” *Reviews of Plasma Physics* **4** pp. 23–91 (1966).
- [20] A. V. Gurevich, “Distribution of captured particles in a potential well in the absence of collisions,” *Soviet Physics JETP* **26** pp. 575–580 (1968).
- [21] E. Buckingham, “On physically similar systems; illustrations of the use of dimensional equations,” *Physical Review* **4** pp. 345–376 (1914).
- [22] P. Helander and D. J. Sigmar, *Collisional Transport in Magnetized Plasmas*, vol. 4 of *Cambridge Monographs on Plasma Physics*, Cambridge University Press (2002), ISBN 978-0-521-02098-5.
- [23] “NIST Digital Library of Mathematical Functions (DLMF),” Release 1.0.17 of 2017-12-22, <http://dlmf.nist.gov/>, F. W. J. Olver, A. B. Olde Daalhuis, D. W. Lozier, B. I. Schneider, R. F. Boisvert, C. W. Clark, B. R. Miller, and B. V. Saunders, editors.
- [24] C. C. Lin and L. A. Segel, *Mathematics Applied to Deterministic Problems in the Natural Sciences*, vol. 1 of *Classics in Applied Mathematics*, SIAM (1988), ISBN 0-89871-229-7.
- [25] R. D. Hazeltine, P. Helander, and P. J. Catto, “Plasma transport near the separatrix of a magnetic island,” *Physics of Plasmas* **4** pp. 2920–2927 (1997).
- [26] T. Fülöp, I. Pusztai, and P. Helander, “Collisionality dependence of the quasilinear particle flux due to microinstabilities,” *Physics of Plasmas* **15**, 072308 (2008).

- [27] S. Takeuchi, “New particle accelerations by magnetized plasma shock waves,” *Physics of Plasmas* **12**, 102901 (2005).

Appendix A

Other shock properties

In this appendix a couple more properties of the shock is presented. These properties only play a very minor role in the thesis, but they might be useful for other studies of electrostatic shocks.

A.1 Ion reflection

The fraction of ions that are reflected by the shock compared to the number of incoming ions, α_j , is calculated in a way similar to how $n_{j,1}$ from (2.72) was calculated, and is given by

$$\alpha_j = \frac{\int_0^{\nu_0} f_j(\boldsymbol{\nu}, \psi = 0) d\boldsymbol{\nu}}{\int_{-\infty}^0 f_j(\boldsymbol{\nu}, \psi = 0) d\boldsymbol{\nu}} = \frac{\operatorname{erf}\left[\sqrt{\frac{\tau_j}{2}} \mathcal{M}\right] + \operatorname{erf}\left[\sqrt{\frac{\tau_j}{2}} (\sqrt{2\zeta_j \psi_{\max}} - \mathcal{M})\right]}{1 + \operatorname{erf}\left[\sqrt{\frac{\tau_j}{2}} \mathcal{M}\right]}. \quad (\text{A.1})$$

In the limit of high electron temperature, i.e. $\tau_j \gg 1$,

$$\operatorname{erf}\left[\sqrt{\frac{\tau_j}{2}} \mathcal{M}\right] \approx 1, \quad (\text{A.2})$$

and

$$\alpha_j \approx \frac{1}{2} \left\{ 1 + \operatorname{erf}\left[\sqrt{\frac{\tau_j}{2}} \mathcal{M} \left(1 - \sqrt{\frac{2\zeta_j \psi_{\max}}{\mathcal{M}^2}}\right)\right] \right\} = \frac{1}{2} \operatorname{erfc}\left[\sqrt{\frac{\tau_j}{2}} \mathcal{M} (1 - \sqrt{F})\right], \quad (\text{A.3})$$

where

$$F_j := \frac{\zeta_j \psi_{\max}}{\mathcal{M}^2/2} \quad (\text{A.4})$$

is the ratio between the maximum electric energy to the mean kinetic energy of the incoming ions. The higher F_j is the larger α_j will be, and the effect is very dramatic if F_j goes from slightly below 1 to slightly above 1 for large τ_j . This means that an ion species with high ζ_j will have a significantly higher proportion of reflected ions.

A.2 Wavelength

The Sagdeev potentials can, just as in section 2.2.4, be used to calculate the wavelengths of the shock downstream oscillations. Similarly to (2.59), the downstream oscillation wavelength is given by

$$\lambda_{\text{ds}} = \sqrt{2} \int_{\psi_{\text{min}}}^{\psi_{\text{max}}} \frac{d\psi}{\sqrt{-\Psi_{\text{ds}}(\psi, \psi_{\text{max}})}}. \quad (\text{A.5})$$

Also like in section 2.2.4, the upstream electrostatic potential of the shock can be said to have an infinite wavelength. This is because (2.79) guarantees that

$$\Psi_{\text{us}}(\psi = 0, \psi_{\text{max}}) = 0, \quad (\text{A.6})$$

and quasi-neutrality also requires that

$$\left. \frac{\partial \Psi_{\text{us}}}{\partial \psi} \right|_{\psi=0} \equiv \hat{\rho}_{\text{us}}(\psi = 0, \psi_{\text{max}}) = 0. \quad (\text{A.7})$$

This means that

$$\Psi_{\text{us}}(\psi, \psi_{\text{max}}) = \mathcal{O}(\psi^2) \quad (\text{A.8})$$

for small ψ , which by the argument in section 2.2.4 results in the upstream electrostatic potential having an infinite wavelength.